

An interferometric CO survey of luminous submm galaxies

T. R. Greve,^{1,2} F. Bertoldi,³ Ian Smail,⁴ R. Neri,⁵ S. C. Chapman,² A. W. Blain,² R. J. Ivison,^{1,6} R. Genzel,^{7,8} A. Omont,⁹ P. Cox,¹⁰ L. Tacconi⁷ & J.-P. Kneib^{2,11,12}

¹ *Institute for Astronomy, University of Edinburgh, Blackford Hill, Edinburgh EH9 3HJ, UK.*

² *California Institute of Technology, Pasadena, CA 91125, USA.*

³ *Max-Planck Institut für Radioastronomie (MPIfR), Bonn, Germany.*

⁴ *Institute for Computational Cosmology, University of Durham, South Road, Durham DH1 3LE, UK.*

⁵ *Institut de Radio Astronomie Millimétrique (IRAM), St Martin d'Hères, France.*

⁶ *Astronomy Technology Centre, Royal Observatory, Blackford Hill, Edinburgh EH9 3HJ, UK.*

⁷ *Max-Planck Institut für extraterrestrische Physik (MPE), Garching, Germany.*

⁸ *Department of Physics, University of California, Berkeley, USA.*

⁹ *Institut d'Astrophysique de Paris, CNRS, Université de Paris, Paris, France.*

¹⁰ *Institut d'Astrophysique Spatiale, Université de Paris Sud, Orsay, France.*

¹¹ *Observatoire Midi-Pyrénées, UMR5572, 14 Avenue Edouard Belin, 31400 Toulouse, France.*

¹² *Laboratoire d'Astrophysique de Marseille, UMR 6110, CNRS-Universit de Provence, Traverse du Siphon-Les trois Lucs, 13012 Marseille, France.*

Accepted ... ; Received ... ; in original form ...

ABSTRACT

In this paper we present results from an IRAM Plateau de Bure millimetre-wave Interferometer (PdBI) survey for CO emission towards radio-detected submillimetre galaxies (SMGs) with known optical and near-infrared spectroscopic redshifts. Five sources in the redshift range $z \sim 1\text{--}3.5$ were detected, nearly doubling the number of SMGs detected in CO. We summarise the properties of all 12 CO-detected SMGs, as well as 6 sources not detected in CO by our survey, and use this sample to explore the bulk physical properties of the SMG population as a whole. The median CO line luminosity of the SMGs is $\langle L'_{\text{CO}} \rangle = (3.8 \pm 2.0) \times 10^{10} \text{ K km s}^{-1} \text{ pc}^2$. Using a CO-to-H₂ conversion factor appropriate for starburst galaxies, this corresponds to a molecular gas mass $\langle M(\text{H}_2) \rangle = (3.0 \pm 1.6) \times 10^{10} M_{\odot}$ within a $\sim 2 \text{ kpc}$ radius, about four times greater than the most luminous local ultraluminous infrared galaxies (ULIRGs) but comparable to that of the most extreme high-redshift radio galaxies and QSOs. The median CO FWHM linewidth is broad, $\langle \text{FWHM} \rangle = 780 \pm 320 \text{ km s}^{-1}$, and the SMGs often have double peaked line profiles, indicative of either a merger or a disk. From their median gas reservoirs ($\sim 3 \times 10^{10} M_{\odot}$) and star-formation rates ($\gtrsim 700 M_{\odot} \text{ yr}^{-1}$) we estimate a lower limit on the typical gas-depletion time scale of $\gtrsim 40 \text{ Myr}$ in SMGs. This is marginally below the typical age expected for the starbursts in SMGs, and suggests that negative feedback processes may play an important role in prolonging the gas consumption time scale. We find a statistically-significant correlation between the far-infrared and CO luminosities of the SMGs which extends the observed correlation for local ULIRGs to higher luminosities and higher redshifts. The non-linear nature of the correlation implies that SMGs have higher far-infrared to CO luminosity ratios, and possibly higher star-formation efficiencies, than local ULIRGs. Assuming a typical CO source diameter of $\theta \sim 0''.5$ ($D \sim 4 \text{ kpc}$), we estimate a median dynamical mass of $\langle M_{\text{dyn}} \rangle \simeq (1.2 \pm 1.5) \times 10^{11} M_{\odot}$ for the SMG sample. Both the total gas and stellar masses imply that SMGs are very massive systems, dominated by baryons in their central regions. The baryonic and dynamical properties of these systems mirror those of local giant ellipticals and are consistent with numerical simulations of the formation of the most massive galaxies. We have been able to impose a lower limit of $\gtrsim 5 \times 10^{-6} \text{ Mpc}^{-3}$ to the co-moving number density of massive galaxies in the redshift range $z \sim 2\text{--}3.5$, which is in agreement with results from recent spectroscopic surveys and the most recent model predictions.

Key words: galaxies: starburst – galaxies: formation – cosmology: observations – cosmology: early Universe

1 INTRODUCTION

The discovery of extragalactic carbon monoxide (CO) rotational line emission (Rickard et al. 1975) and, in particular, the

first detections of CO at cosmologically significant redshifts in IRAS F10214+4724 at $z = 2.29$ (Brown & Vanden Bout 1991; Solomon, Downes & Radford 1992a), the Cloverleaf at $z = 2.56$ (Barvainis et al. 1994) and BRI 1202–0725 at $z = 4.69$ (Omont et al. 1996) revealed the potential of CO as a tracer of molecular gas in the early Universe. Since those pioneering efforts, progress has been slow due to the severe observational obstacles: the faintness of the CO emission, except for cases where the source is gravitationally magnified; inaccurate spectroscopic redshifts coupled with the small instantaneous bandwidth of most modern-day correlators; and in some cases, an unfortunate combination of redshift and available receiver coverage, as well as atmospheric transparency, at millimetre wavelengths. As a result only 30-or-so $z > 1$ objects have been detected to date, most of which have been extremely luminous, often gravitationally lensed, QSOs (e.g. Omont et al. 1996; Guilloteau et al. 1997, 1999; Downes et al. 1999; Cox et al. 2002; Bertoldi et al. 2003; Beelen et al. 2004) and high-redshift radio galaxies (HzRGs — e.g. Papadopoulos et al. 2000; De Breuck et al. 2003a).

The slow increase in the number of CO detections contrasts with the rapid growth in samples of high-redshift galaxies selected through continuum observations at submillimetre (submm) wavelengths, which detect thermal emission from dust. The advent of large-format submm/mm cameras, SCUBA (Holland et al. 1999) and MAMBO (Kreysa et al. 1998), revealed the presence of a significant population of dust-enshrouded, and therefore hitherto undetected, galaxies at high redshifts (e.g. Smail, Ivison & Blain 1997; Barger, Cowie & Sanders 1999; Bertoldi et al. 2000). Today such observations are routine, and several hundred submm-selected (or SCUBA) galaxies (SMGs) have been discovered (e.g. Blain et al. 2002; Scott et al. 2002; Webb et al. 2003; Borys et al. 2003).

Until recently, only two SMGs had been detected in CO (Frayer et al. 1998, 1999; Downes & Solomon 2003; Genzel et al. 2003), largely owing to the extreme faintness of SMGs in the optical and the difficulties in obtaining reliably spectroscopic redshifts. However, a major step forward was made by Chapman et al. (2003b, 2005) who used the highly-efficient, blue-sensitive LRIS-B spectrograph on the Keck Telescope to obtain spectroscopic redshifts for a large sample of SMGs. This motivated a major survey at the IRAM Plateau de Bure Interferometer (PdBI) to look for CO emission from this high-redshift sample. The observational cycle involves: identifying a robust radio counterpart to an SMG in deep VLA radio maps (see e.g. Ivison et al. 2002); placing a LRIS-B/Keck slit on this position to obtain a spectroscopic redshift (Chapman et al. 2003b, 2005); frequently confirming the redshift in the near-infrared, usually via redshifted H α (Simpson et al. 2004; Swinbank et al. 2004); and, finally, searching for redshifted CO emission with PdBI. The initial results from this CO programme were described in Neri et al. (2003). Although an expensive process in terms of telescope time, this is currently the only feasible and effective route for detecting CO from SMGs.

CO observations can potentially provide unique information about the enigmatic SMG population. First and foremost, CO traces the bulk of the molecular gas in SMGs: the high-level ($J \geq 2$) transitions arise in the warm and dense gas while lower level J lines probe the quiescent and likely cooler gas which may lurk in the outskirts of SMGs. Detecting and mapping this molecular emission enables us to precisely determine the spatial and kinematic location of the gas-rich components within an SMG. About two-thirds of SMGs are found to be large, morphologically complex systems in the optical/near-infrared and/or the radio, with typically one or more companions (e.g. Smail et al. 1999; Ivison et al. 2002;

Chapman et al. 2003c, 2004). For example, in one SMG, Neri et al. (2003) identified CO emission coincident with a second, fainter radio source $\sim 4''$ away from the radio counterpart for which the spectroscopic redshift had been found. Secondly, CO observations yield fairly accurate estimates of the amount of molecular gas available to fuel the starburst and/or the AGN responsible for the large far-infrared luminosities. While the conversion factor between the CO luminosity and molecular gas mass is uncertain, CO observations clearly provide a much better constraint on the amount of gas present in SMGs than the estimates based on submm continuum observations and an adopted spectral energy distribution (SED) and gas-to-dust ratio.

The first two CO detections of SMGs revealed the presence of copious amount of molecular gas ($\sim 10^{10} M_{\odot}$), suggesting that intense star formation is occurring in these systems (Frayer et al. 1998, 1999). Furthermore, from a reliable estimate of the gas reservoir in an SMG we can say something about the gas exhaustion time-scale, i.e. the duration of the submm-luminous phase. This, in turn, allows us to make an educated guess about the possible descendants of SMGs, and thus place them in an evolutionary context with other high- and low-redshift galaxy populations.

Observations of the shape and width of CO lines also provides important information about the kinematics in SMGs (Neri et al. 2003; Tacconi et al. 2005). In particular, if the CO emission is spatially resolved we can use that, in conjunction with the width of the line profile, to constrain the dynamical mass of the host galaxy. Estimates of the dynamical mass based on CO are likely to be ‘cleaner’ than estimates from optical/near-infrared spectroscopy, which are prone to extinction by dust and the effects of non-gravitational motions in the emitting gas, such as outflows. The best example of resolved CO emission in a SMG (Genzel et al. 2003) shows gas extended on scales of $\sim 3\text{--}5$ kpc and that most of the dynamical mass ($\sim 3 \times 10^{11} M_{\odot}$) is baryonic. Such large, widely-distributed gas reservoirs suggest that the brightest SMGs are not merely high-redshift replicas of the local population of ULIRGs. However, a representative picture of the gas distribution in SMGs will have to await high-resolution CO observations of a large sample of SMGs.

Since CO observations provide a means of ‘weighing’ galaxies at high redshifts, both in terms of their baryonic gas mass content and their total dynamical mass, they can be used to help piece together a picture of the mass assembly of massive galaxies in the early Universe. In the classical cold-dark matter (CDM) scenario of structure formation (White & Frenk 1991), massive spheroidal galaxies are the end products of a gradual build-up of mass via merging and, as a result, form late in the history of the Universe. However, as pointed out by Genzel et al. (2003), at least some SMGs appear to be massive, baryon-dominated galaxies already at $z \sim 2\text{--}3$. The discovery of massive, evolved early-type galaxies at $z \gtrsim 1.5$ (e.g. Cimatti et al. 2004), which could be the descendants of $z \gtrsim 2$ SMGs, suggests that some massive spheroids were not formed at $z \lesssim 1$. In fact, if the brightest 25 per cent of the SMGs are massive baryonic systems, then their abundance indicates that the build up of massive galaxies in the early Universe was much faster than previously expected, and could pose a serious challenge for current models of gas processing in galaxy formation (e.g. Cole et al. 1994; Kauffmann et al. 1999; Baugh et al. 2004).

In this paper we present the most recent results from a systematic survey of CO emission towards radio-identified SMGs with spectroscopic redshifts in the range $z \sim 1\text{--}3.5$ (corresponding to 40–10% of the age of the Universe at the respective epochs), and use these to address the issues outlined above. This is part of a

major effort currently being undertaken at the PdBI with the aim of detecting and imaging CO emission towards ~ 20 – 30 SMGs. In §2 and 3 we describe the observations and derive properties for each new source observed. In §4 we define a sample of 12 sources consisting of all SMGs detected in CO to date, from which the average physical properties of the bright SMG population are derived. We discuss their properties and compare with those of other galaxy populations in §5. Finally, §6 discusses the impact of our observations on models of galaxy formation and evolution. Throughout we adopt a flat cosmology, with $\Omega_m = 0.27$, $\Omega_\Lambda = 0.73$ and $H_0 = 71 \text{ km s}^{-1} \text{ Mpc}^{-1}$ (Spergel et al. 2003).

2 OBSERVATIONS

In total, 11 SMGs were targeted for CO observations with PdBI (see Table 1), drawn from five independent submm surveys: the SCUBA Lens Survey (SMMJ02396–0134 — Smail, Ivison & Blain 1997); the Hubble Deep Field (SMMJ12360+6210 — Chapman et al. 2003a); the Hawaii Survey Fields, SSA 13 and SSA 22 (SMMJ13120+4242, SMMJ13123+4239 — Chapman et al. 2005; SMMJ22174+0015 — Barger, Cowie & Sanders 1999); The SCUBA UK 8mJy Survey of the Lockman Hole East and ELAIS N2 (SMMJ10523+5722, SMMJ10524+5724, SMMJ16363+4055, SMMJ16363+4056, and SMMJ16366+4105 — Scott et al. 2002); and a 1200- μm MAMBO survey of the same two fields (SMMJ16371+4053¹ — Greve et al. 2004b).

Deep radio imaging was used to identify radio counterparts to all the targeted SMGs and accurately locate these relative to optical/near-infrared reference fields (Smail et al. 1999; Chapman et al. 2003a; Ivison et al. 2002). Subsequent spectroscopy with Keck/LRIS-B (Oke et al. 1995) and CFHT/OSIS-V in the case of SMMJ02396–0134 (Soucail et al. 1999) provided UV spectroscopic redshifts for all sources (see Chapman et al. 2003b, 2005). A subset of the sample were spectroscopically observed in the near-infrared to provide more reliable systemic redshifts from the wavelengths of redshifted H α or [OIII] $\lambda 5007\text{\AA}$ emission lines (Swinbank et al. 2004) to aid in our search for redshifted CO emission. Here, and for the remainder of this paper, we take the systemic redshift to be equivalent to the CO redshift.

From our sample of 11 sources, 10 were part of our statistically-complete CO survey and were targeted during two observing campaigns, during the winter of 2002–03 and the summer of 2003, in good to excellent weather. The observations were done in D configuration in order to maximise the sensitivity, and used five of the six available antennae, giving a total of 10 baselines. We stress that the survey is on-going and that the 10 sources reported here are merely those which were observed during the 2003 season. In addition, we included an 11th source, SMMJ02396–0134, for which data was originally obtained by J.-P. Kneib and G. Soucail during summer/autumn of 1999, and these were retrieved from the PdBI data archive. Observations of this source were done in D and C configuration. The details of the observations of all 11 sources are summarised in Table 1.

While our main goal was to detect redshifted CO emission in the 3-mm waveband, we also used the 1.3-mm receivers to attempt to determine accurate continuum positions and fluxes or, in cases where a higher- J CO line would coincide with the 1.3-mm band,

Table 1. Log of the PdBI observations for the 11 SMGs analysed in this paper. The on-source integration time (t_{int}) is the observing time for the equivalent six element array.

Source	Observing Dates	t_{int} (hr)	Detection?
SMMJ02396–0134	1999 Jun 20, 24–26, 29, Aug 24, 27, Sep 7	7.4	Y
SMMJ10523+5722	2003 Apr 25, May 06	16.6	N
SMMJ10524+5724	2003 Mar 27	3.9	N
SMMJ12360+6210	2003 Jun 01, 03, 18, Aug 30, Sep 01	9.4	N
SMMJ13120+4242	2003 May 17, 22–23, 26	9.2	Y
SMMJ13123+4239	2003 Jun 23, 26, 27	4.7	N
SMMJ16363+4055	2003 Mar 31, Apr 03, 21	11.2	N
SMMJ16363+4056	2003 Aug 11, 22, 24	9.6	N
SMMJ16366+4105	2003 Apr 13–14, 23, May 1	14.9	Y
SMMJ16371+4053	2003 Jul 25–26, 29 Aug 1, 2, Sep 4	17.1	Y
SMMJ22174+0015	2003 May 9–13, 29–30, Jun 4, Sep 12, 14	17.3	Y

to search for emission from this transition, e.g. SMMJ04431+0210 (Neri et al. 2003). To achieve our goals the correlators were configured for line and continuum observations and simultaneously covered 580 MHz in the 3-mm and 1.3-mm bands: this corresponds to a typical velocity coverage of 1700 and 750 km s^{-1} at 3 and 1.3 mm, respectively.

Where a near-infrared spectroscopic redshift was unavailable we have to correct for the likely systematic blueshifts of UV line features relative to the CO emission. We therefore tuned the 3-mm receivers slightly redward of the measured spectroscopic redshift. This meant that for a typical redshift uncertainty of $\Delta z = 0.005$, any source at $z \geq 1$ would have its CO line peak fall within $0.5 \times 580 \text{ MHz} = 290 \text{ MHz}$ of the 3-mm band centre. In a few instances, a line was detected at the edge of the band pass. The frequency setting was then adjusted to centre the line in the bandpass, and the source was re-observed. A source was typically observed for 2–3 tracks (10–18 hrs). If no signal had been detected after this, the source was not pursued further.

All data reduction employed the IRAM GILDAS software (Guilloteau & Lucas 2000). This involved careful monitoring of the quality of the data throughout a track, and subsequent flagging of any bad and high phase-noise visibilities. For passband calibration we typically used one or more bright quasars. Phase and amplitude variations within each track were calibrated out by inter-leaving reference observations of nearby fainter quasars every 20 m. In the best conditions, the typical rms phase noise per baseline at 3 mm was $\lesssim 10^\circ$, increasing to $\lesssim 40^\circ$ in the worst cases. Observations of the primary calibrators, 3C454.3, 3C345, 3C273, and MWC 349, were used to determine the flux scale. Finally, naturally weighted data cubes were created using GILDAS.

3 THE SOURCES

No sources were detected at 1.3-mm, and the data were of so poor quality that even upper limits were useless. For the remainder of this paper we shall therefore only discuss the 3-mm data. For each source the continuum level at 3-mm was estimated by extrapolating from its submm flux and assuming a spectral index of $\beta = 1.5$. In all cases we find the contribution from the continuum emission to the CO line at 3-mm to be less than $\lesssim 5$ per cent, and therefore negligible. Of the 11 sources whose observations are analysed in this paper, CO emission was reliably detected in five. Including the

¹ This source was denoted MMJ16371+4053 in Greve et al. (2004b)

first three (out of three) detections from our survey from Neri et al. (2003) yields a detection rate of 57% (8/14) to date.

The failure to detect CO in some of our sources is unlikely to be due to the optical redshift being wrong, since the quality of the spectra is generally high (Chapman et al. 2005). Similarly, the possibility that the identification is wrong, and therefore the redshift is for the wrong object, appears to be remote given the excellent correspondence between the radio and submm (e.g. Ivison et al. 2002), and the extremely small likelihood of finding a $z \sim 2$ galaxy at that position, which is not related to the submm emission. Instead we feel the explanation for the missing CO emission is due to either too large a velocity offset between the CO and optical emission (putting the former outside our selected correlator coverage, see §4.2), a CO line with a width comparable to our correlator bandwidth, or simply that the sources are too faint in CO to be detected in the given integration time. In the latter case, the 6 non-detections can provide useful upper limits on their CO luminosity and gas masses and as a result we have included them in the analysis in this paper.

In remainder of this section we shall briefly describe the properties of the five SMGs for which new CO detections are presented in this paper as well as the 6 non-detections.

SMMJ02396–0134 The CO(2–1) spectrum of SMMJ02396–0134 is shown in Fig. 1a. The blue wing of the line is missing due to the limited correlator bandwidth available in 1999, but nonetheless it is evident that the line is double peaked. The CO redshift, $z_{\text{CO}} = 1.062 \pm 0.002$, was defined as the flux-weighted redshift, see section 4.2 for details. The widths of the two peaks were estimated by simultaneously fitting two Gaussians to the spectrum, which yielded FWHM values $180 \pm 20 \text{ km s}^{-1}$ and $430 \pm 50 \text{ km s}^{-1}$ for the blue-shifted and red-shifted peaks, respectively. The velocity offsets of the two peaks were -280 km s^{-1} and 90 km s^{-1} , respectively, measured relative to the CO redshift. From the double Gaussian fit the velocity-integrated CO(2–1) line flux is $I_{\text{CO}} = 3.4 \pm 0.3 \text{ Jy km s}^{-1}$. A single Gaussian fit to the line profile leads to a FWHM value of $780 \pm 60 \text{ km s}^{-1}$. Due to the truncated line we can only impose a lower limit $\simeq 870 \text{ km s}^{-1}$ on the full width at zero intensity (FWZI).

The emission integrated over the line from -460 km s^{-1} to 110 km s^{-1} is shown as contours overlaid on a K -band image in Fig. 2a. The emission is detected at $\geq 10\sigma$, where $\sigma = 0.40 \text{ mJy beam}^{-1}$, and coincides with the optical/near-infrared counterpart to within the relative astrometrical errors. The source appears extended in the north-south direction, and an elliptical Gaussian fit to the CO emission in the image plane yields a source size of $9''.5 \times 5''.5$, which is slightly larger than the $8''.3 \times 5''.3$ synthesized beam. The two velocity components of the source have a slight spatial offset, with the blue-shifted peak (integrated from -460 to -120 km s^{-1}) $1.2''$ north of the centroid of the integrated line emission and the red-shifted peak (integrated from -120 to 110 km s^{-1}) offset $0.3''$ east and $1.6''$ south of the central position. The positional uncertainties in the maps are $0.3\text{--}0.4''$, suggesting that the observed offsets are significant.

SMMJ13120+4242 The CO(4–3) spectrum of SMMJ13120+4242 is shown in Fig. 1e. A single Gaussian provides an excellent fit to the data, as measured by the χ^2 statistic, and yields a velocity-integrated flux density, $1.7 \pm 0.3 \text{ Jy km s}^{-1}$ and a line width of FWHM $\simeq 530 \pm 50 \text{ km s}^{-1}$. We find a systemic CO redshift of $z_{\text{CO}} = 3.408 \pm 0.002$.

The velocity-integrated CO(4–3) emission yields a $\gtrsim 6\text{-}\sigma$ detection ($\sigma = 0.32 \text{ mJy beam}^{-1}$) at position which is offset $0.8''$ to the north-east of the optical counterpart (Fig. 2b). The positional

error is $\sim 1''$, and so the offset is not significant. The CO emission is unresolved.

SMMJ16366+4105 The CO(3–2) spectrum of SMMJ16366+4105 (Fig. 1i) is very broad with the blue edge of the line ending abruptly. The spectrum exhibits a double-peaked line similar to SMM02396–0134, although less distinct. The CO redshift is $z = 2.450 \pm 0.002$. A simultaneous fit of two Gaussians provides a superior fit to the spectrum than a single Gaussian, and places the blue-shifted and red-shifted peaks at velocity offsets of -270 km s^{-1} and $+210 \text{ km s}^{-1}$, respectively. The velocity-integrated line flux is $I_{\text{CO}} = 1.8 \pm 0.3 \text{ Jy km s}^{-1}$. A single Gaussian fitted to the spectrum yields a line width FWHM $= 870 \pm 80 \text{ km s}^{-1}$ – the second largest line width of the sample.

The integrated CO emission, shown in Fig. 2c, is detected at the $\gtrsim 8\text{-}\sigma$ level ($\sigma = 0.21 \text{ mJy beam}^{-1}$), and coincides with the radio and faint optical/near-infrared counterpart. We imaged the blue-shifted and red-shifted peaks separately, using different velocity cut-offs, in order to look for positional offsets between the two, but found no evidence for a velocity gradient across the source. It is possible that part of the CO emission is related to the faint near-infrared source $\sim 2''$ south-west of the CO centroid, the compact radio counterpart displays a similar faint tail of emission in this direction. SMMJ16366+4105 is a prime target for further, higher-resolution CO observations.

SMMJ16371+4053 The detection of CO(3–2) towards SMMJ16371+4053 is the first for a MAMBO-selected source. The CO(3–2) line profile is shown in Fig. 1j. The flux-weighted, systemic CO redshift is $z_{\text{CO}} = 2.380 \pm 0.004$. While clearly detected, the poor signal-to-noise ratio prevents us from defining the line profile, except to say that the line appears broad with FWZI $\gtrsim 900 \text{ km s}^{-1}$. A Gaussian fit yields a formal line width of FWHM $\sim 830 \text{ km s}^{-1}$ and a velocity-integrated line flux $I_{\text{CO}} = 1.0 \pm 0.2 \text{ Jy km s}^{-1}$.

The integrated emission is shown in Fig. 1d. The source is detected at $\gtrsim 5\sigma$ ($\sigma = 0.18 \text{ mJy beam}^{-1}$) and coincides with the optical/near-infrared counterpart to within the positional errors.

SMMJ22174+0015 The CO(3–2) spectrum of this source shown in Fig. 1l is the weakest of our detections. After heavily binning the spectrum, we estimate the line to be significant at the $\gtrsim 4\text{-}\sigma$ level. We measure the flux-weighted, systemic CO redshift as $z_{\text{CO}} = 3.099 \pm 0.004$. A Gaussian fit to the spectrum yields a line width of FWHM $= 780 \pm 100 \text{ km s}^{-1}$ and a line flux density of $I_{\text{CO}} = 0.8 \pm 0.2 \text{ Jy km s}^{-1}$.

Contours of the velocity-integrated CO emission are shown on a K -band image in Fig. 2e. The CO emission is detected at the $\sim 4.7\text{-}\sigma$ level ($\sigma = 0.17 \text{ mJy beam}^{-1}$), at a position offset by $\sim 2.5''$ north-west from the optical counterpart, but only $\sim 0.8''$ away from the radio position (phase centre).

Non-detections In Table 2 we list the 3σ upper limits on the 3-mm CO line flux spatially coincident with the radio position as well as the redshift range searched for each of the 6 non-detections. The upper limits were calculated using the equation $I_{\text{CO}} = 3\sigma (\delta v \Delta v_{\text{FWHM}})^{1/2}$, where σ is the channel-to-channel rms noise, δv the velocity resolution and Δv_{FWHM} the line width (see e.g. Seaquist, Ivison & Hall 1995). In our calculation of the upper limits we used the rms noise in the spectra binned to 100 MHz resolution and adopted a line width of 500 km s^{-1} . The integrated CO (3–2) map of SMMJ12360+6210 shows a $\sim 4\sigma$ peak slightly eastwards of the phase-centre, and is thus possibly another tentative detection, albeit marginal. In the remaining cases no line emission is observed at a significance $\geq 3\sigma$.

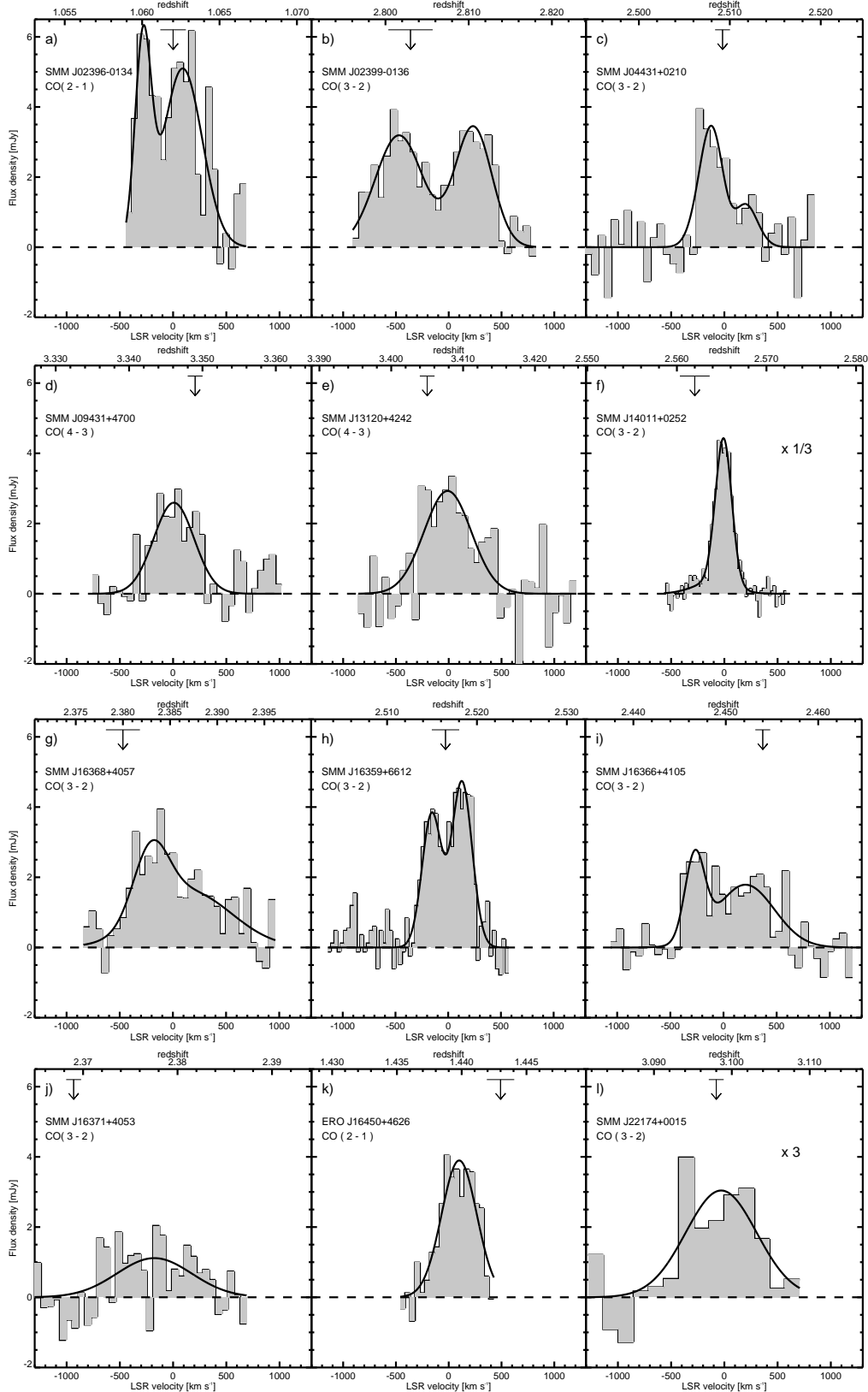


Figure 1. CO line profiles of the 12 SMGs detected in CO to date. The profiles have been plotted on similar flux- and velocity-scales in order to facilitate an easy comparison between individual sources, to achieve this the spectra of SMM J14011+0252 and SMM J22174+0015 have been scaled by a factor $\times 1/3$ and $\times 3$, respectively. The LSR velocity-scale is relative to the CO redshift. Optical redshifts are denoted by arrows and the horizontal bars on top of the arrows indicate the uncertainty of the redshifts. The redshifts derived from the CO lines are given in Table 2. The solid curves represent the best-fits to the spectra using either single or double Gaussian profiles. The spectra shown in c), d) and g) are taken from Kneib et al. (2003); h) is taken from Genzel et al. (2003), Downes & Solomon (2003) and Andreani et al. (2000), respectively. The spectra have been binned into 20 MHz bins, except for f), h) and l) where the frequency binning is 7, 10 and 40 MHz, respectively.

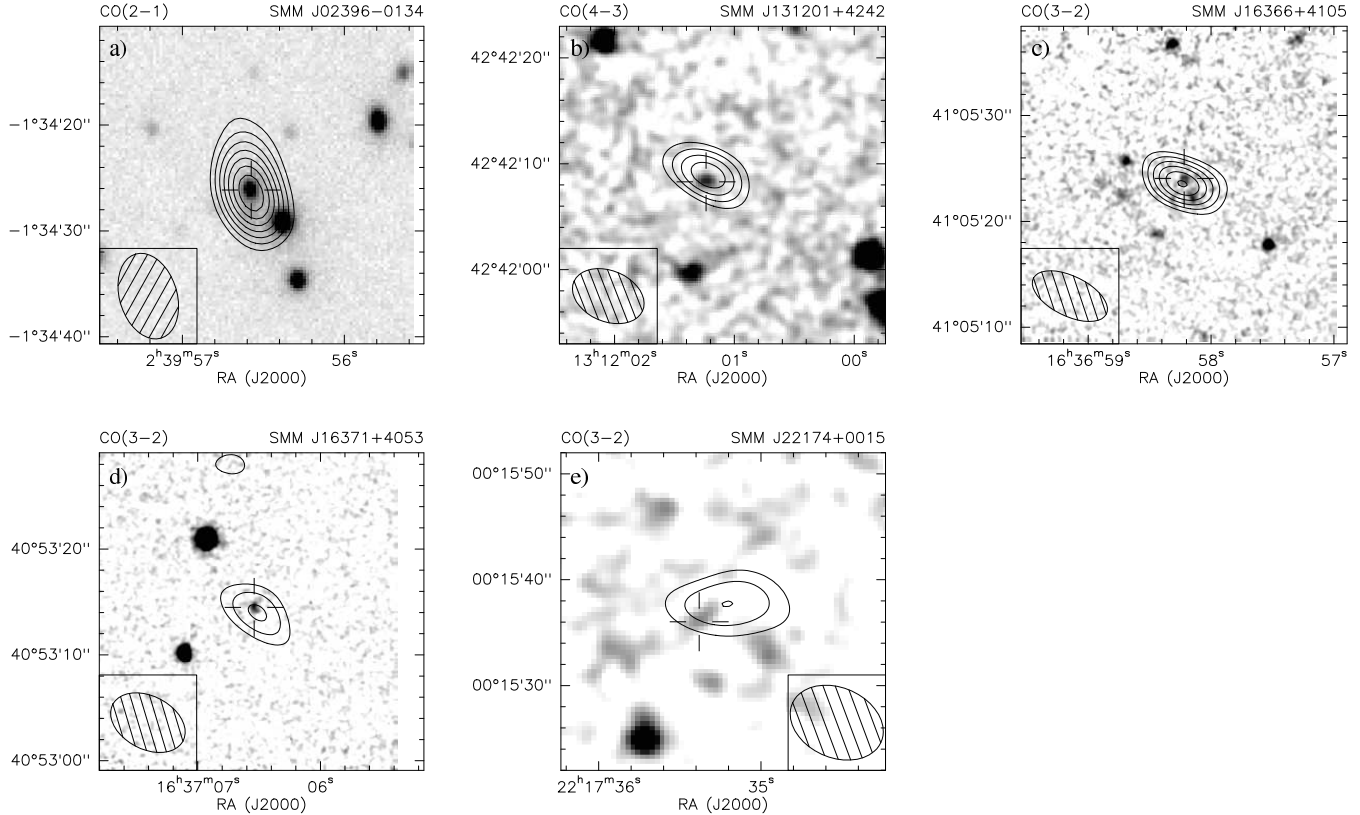


Figure 2. Contours of the velocity integrated CO emission overlaid on $30'' \times 30''$ K -band images of the five new CO-detected SMGs presented in this paper. The K -band images are centred on the radio positions, while the open crosses mark the position of the optical/near-infrared counterparts for which the spectroscopic redshifts were obtained. In all panels the contours start at 3σ and increase in steps of 1σ , where $\sigma = 0.40, 0.32, 0.21, 0.18$, and 0.17 mJy beam $^{-1}$ in panels a), b), c), d), and e), respectively. The synthesized beams are (panels a) to e), shown as hatched ellipses) $8''.3 \times 5''.3$ at position angle 15° (east of north), $6''.9 \times 4''.8$ at 66° , $7''.4 \times 3''.9$ at 62° , $7''.4 \times 5''.0$ at 61° , and $9''.0 \times 6''.6$ at 65° . The (1σ) uncertainties on measured positions in the optical and mm frames are $\lesssim 0''.1$ and $\lesssim 0''.3$, respectively. The K -band data for a), b) and e) were published in Smail et al. (2002), Smail et al. (2004) and Chapman et al. (2003a), respectively, while c) and d) were published in Ivison et al. (2002).

4 SAMPLE PROPERTIES

4.1 The sample

The main goal of this paper is to assemble a large sample of SMGs observed in CO. In order to achieve this, we add to the 11 new sources in Table 1 from our survey (detections as well as non-detections) and the three earlier CO detections from this survey described in Neri et al. (2003), the three SMGs detected in CO prior to our survey: SMM J02399-0136 (Frayser et al. 1998; Genzel et al. 2003), SMM J14011+0252 (Frayser et al. 1999; Downes & Solomon 2003) and SMM J16359+6612 (Sheth et al. 2004; Kneib et al. 2004). The latter is a triply-imaged lensed galaxy with CO detected towards all three components, and in Fig. 1h we have displayed the combined (and therefore highest signal-to-noise) spectrum of all three components as given in Kneib et al. (2004). For the velocity-integrated line flux we have adopted the value of the component with the strongest detection, i.e. component B (Kneib et al. 2004) – see Table 2.

We also include the extremely red object, HR 10, at $z = 1.443$ (ERO J16450+4626; Hu & Ridgway 1994). Initially studied because of its extremely red optical–near-infrared colours, subsequent observations with SCUBA and *Hubble Space Telescope* revealed that HR 10 is a powerful SMG with a distorted rest-frame UV morphology (e.g. Cimatti et al. 1998; Dey et al. 1999). Hence, HR 10

bears all the characteristics of a SMG and would have been detected in any of the SCUBA surveys to date. The CO(5–4), CO(2–1) and CO(1–0) lines have all been detected towards this source (Andreani et al. 2000; Greve et al. 2003).

Finally, we note that Hainline et al. (2004) detected CO(3–2) towards the submm source SMM J04135+10277, the first type-1 QSO to be selected at submm wavelengths (Knudsen, van der Werf & Jaffe 2003), as part of an Owens Valley Millimeter Array survey of CO emission towards high-redshift QSOs. SMM J04135+10277 is not only one of the brightest submm sources known but also an extremely luminous CO source. While SMM J04135+10277 was discovered in a blank-field (albeit lensing-assisted) submm survey and thus meets the selection criteria for our sample, only about 3 per cent of radio-identified SMGs are broad-line QSOs (Chapman et al. 2005), suggesting that this source is not representative of the SMG population as a whole. SMM J04135+10277 is therefore not included in our sample of CO-detected SMGs.

The final SMG sample consists of 12 CO detections and 6 non-detections, their observational properties are listed in Table 2. The CO line profiles of the 12 detected sources are shown in Fig. 1. In the following sections we shall use the CO observations to investigate the physical properties of the SMG population, see Table 3. In the case where a SMG is known to be gravitationally-lensed, we have corrected the luminosities, gas masses, and linear sizes, etc.,

Table 2. SMGs observed in CO to date, including the submm-bright ERO J16450+4626 which although not selected in the submm is thought to be similar to the SMG population. The top section of the table lists the five new CO detections presented here and the three previously published detections from our survey (Neri et al. 2003); the 6 non-detected SMGs are listed in the middle section, while the sources from the literature are given in the bottom section of the table.

Source name	Transition	CO position		Optical/NIR position		Radio position		z_{spec}	z_{CO}	ΔV_{FWHM}	I_{CO}	Ref.
		α_{J2000} (h m s)	δ_{J2000} ($^{\circ}$ ' ")	α_{J2000} (h m s)	δ_{J2000} ($^{\circ}$ ' ")	α_{J2000} (h m s)	δ_{J2000} ($^{\circ}$ ' ")			(km s $^{-1}$)	(Jy km s $^{-1}$)	
Detections												
SMM J02396−0134 ^{a,b}	(2−1)	02 39 56.59	−01 34 26.6	02 39 56.51	−01 34 25.66	02 39 56.30	−01 34 30.8	1.062 ± 0.001 ^c	1.062 ± 0.002	780 ± 60	3.4 ± 0.3	[1]
SMM J13120+4242	(4−3)	13 12 01.20	+42 42 08.8	13 12 01.23	+42 42 08.2	13 12 01.17	+42 42 08.1	3.405 ± 0.001 ^d	3.408 ± 0.002	530 ± 50	1.7 ± 0.3	[1]
SMM J16366+4105	(3−2)	16 36 58.23	+41 05 23.7	16 36 58.21	+41 05 23.9	16 36 58.19	+41 05 23.8	2.454 ± 0.001 ^d	2.450 ± 0.002	870 ± 80	1.8 ± 0.3	[1]
SMM J16371+4053	(3−2)	16 37 06.50	+40 53 13.8	16 37 06.54	+40 53 14.1	16 37 06.51	+40 53 13.8	2.374 ± 0.001 ^d	2.380 ± 0.004	830 ± 130	1.0 ± 0.2	[1]
SMM J22174+0015	(3−2)	22 17 35.20	+00 15 37.6	22 17 34.95	+00 15 33.2	22 17 35.15	+00 15 37.2	3.098 ± 0.002 ^d	3.099 ± 0.004	780 ± 100	0.8 ± 0.2	[1]
SMM J04431+0210 ^{a,b}	(3−2)	04 43 07.25	+02 10 23.3	04 43 07.25	+02 10 24.4	04 43 07.25	+02 10 24.4	2.5092 ± 0.0008 ^e	2.5094 ± 0.0002	350 ± 60	1.4 ± 0.2	[2]
	(7−6)	≤ 0.8	[2]
SMM J09431+4700 ^a	(4−3)	09 43 03.74	+47 00 15.3	09 43 03.70 ^f	+47 00 15.1 ^f	09 43 03.7	+47 00 15.1	3.349 ± 0.001 ^d	3.3460 ± 0.0001	420 ± 50	1.1 ± 0.1	[2]
	(9−8)	≤ 1.0	[2]
SMM J16368+4057	(3−2)	16 36 50.43	+40 57 34.7	16 36 50.40	+40 57 34.2	16 36 50.43	+40 57 34.5	2.380 ± 0.002 ^d	2.3853 ± 0.0014	840 ± 110	2.3 ± 0.2	[2]
	(7−6)	16 36 50.41	+40 57 34.3	2.383 ± 0.002	...	1.1 ± 0.2	[2]
Non-detections												
SMM J10523+5722	(3−2)	10 52 30.75	+57 22 09.4	10 52 30.73	+57 22 09.5	2.611 ± 0.001 ^d	2.5901 − 2.6119	...	≤ 0.6 ^g	[1]
SMM J10524+5724	(3−2)	10 52 38.34	+57 24 36.0	10 52 38.30	+57 24 35.8	3.036 ± 0.001 ^d	3.0593 − 3.0318	...	≤ 1.0 ^g	[1]
SMM J12360+6210	(3−2)	12 36 00.12	+62 10 47.7	12 36 00.20	+62 10 47.0	1.994 ± 0.001 ^d	1.9865 − 2.0015	...	≤ 1.3 ^g	[1]
SMM J13123+4239	(3−2)	13 12 32.31	+42 39 49.5	13 12 32.30	+42 39 50.0	2.320 ± 0.001 ^d	2.3115 − 2.3300	...	≤ 1.4 ^g	[1]
SMM J16363+4055	(3−2)	16 36 31.47	+40 55 46.6	16 36 31.47	+40 55 46.9	2.283 ± 0.001 ^d	2.2676 − 2.2919	...	≤ 0.6 ^g	[1]
SMM J16363+4056	(2−1)	16 36 39.16	+40 56 35.9	16 36 39.01	+40 56 35.9	1.495 ± 0.001 ^d	1.4802 − 1.5001	...	≤ 1.4 ^g	[1]
Literature sources												
SMM J02399−0136 ^{a,b}	(3−2)	02 39 51.89	−01 35 58.9	02 39 51.88	−01 35 58.0	02 39 51.88	−01 35 58.0	2.803 ± 0.003 ^d	2.808 ± 0.002	710 ± 80	3.0 ± 0.4	[3]
	(3−2)	02 39 51.87	−01 35 58.8	02 39 51.85	−01 35 58.2	2.8076 ± 0.0002	≥ 1100	3.1 ± 0.4	[4]
SMM J14011+0252 ^{a,b}	(3−2)	14 01 04.92	+02 52 25.6	14 01 04.95	+02 52 24.0	14 01 04.96	+02 52 23.5	2.562 ± 0.002 ^d	2.5653 ± 0.0003	200 ± 40	2.4 ± 0.3	[5]
	(3−2)	14 01 04.93	+02 52 24.1	2.5652 ± 0.0001	190 ± 11	2.8 ± 0.3	[6]
	(7−6)	14 01 04.92	+02 52 23.8	2.5651 ± 0.0002	170 ± 30	3.2 ± 0.5	[6]
SMM J16359+6612 ^{a,b}	(3−2)	16 35 54.15	+66 12 24	16 35 54.19	+66 12 24.9	2.5165 ± 0.0015 ^e	2.5168 ± 0.0003	500 ± 100	3.5 ± 0.1	[7]
	(3−2)	16 35 54.10	+66 12 23.8	2.5174 ± 0.0002	500 ± 100	2.50 ± 0.12	[8]
ERO J16450+4626 ^b	(2−1)	16 45 02.26	+46 26 26.5	16 45 02.36	+46 26 25.5	1.443 ± 0.001 ^e	1.439 ± 0.001	400 ± 20	1.40 ± 0.10	[8]
	(5−4)	1.440 ± 0.001	380 ± 20	1.35 ± 0.10	[9]
	(1−0)	0.6 ± 0.1	[10]

^a The source is lensed, see Table 3 for magnifications μ_L .

^b The CO emission is extended.

^c The redshift is derived from the OII λ 3727 line (Soucail et al. 1999).

^d The redshift is derived from Ly α (Iverson et al. 2000; Ledlow et al. 2002; Smail et al. 2003; Chapman et al. 2005).

^e The redshift is derived from H α (Dey et al. 1999; Frayer et al. 2003; Kneib et al. 2004; Swinbank et al. 2004).

^f Position of H7, see Neri et al. (2003) for details.

^g The 3σ upper limits have been calculated over an assumed velocity range of 500 km s $^{-1}$.

[1] This work; [2] Neri et al. (2003); [3] Frayer et al. (1998); [4] Genzel et al. (2003); [5] Frayer et al. (1999); [6] Downes & Solomon (2003); [7] Sheth et al. (2004); [8] Kneib et al. (2004); [9] Andreani et al. (2000); [10] Greve et al. (2003).

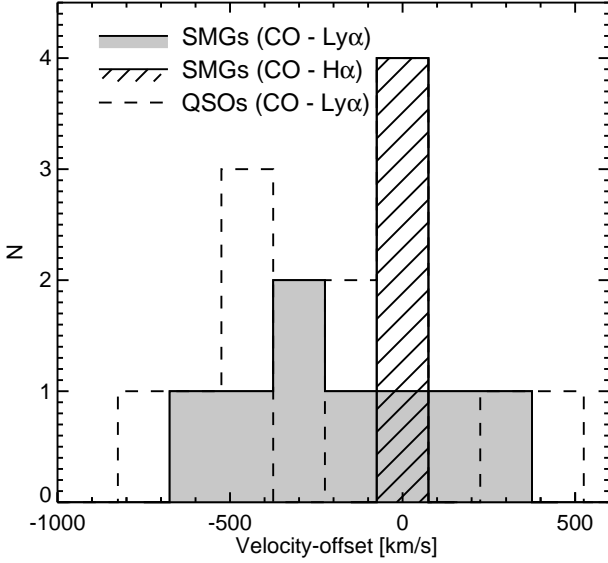


Figure 3. The histograms show the distribution of velocity differences derived from the redshifts from CO line observations and restframe-UV spectroscopy. We show the distribution for the eight SMGs for which spectroscopic redshifts have been derived from the $\text{Ly}\alpha$ line (grey shaded histogram) and for the 15 QSOs in Table 4 (two of the QSOs have velocity-offsets $\lesssim -1000 \text{ km s}^{-1}$). The hashed histogram compares the redshifts between the CO and $\text{H}\alpha$ emission line for the 4 SMGs with redshifts derived from $\text{H}\alpha$ (3) or $[\text{OII}]\lambda 3727 \text{ \AA}$ (1). The bin size is 150 km s^{-1} which also reflects the typical error in the velocity offsets.

using the gravitational lensing magnification factors listed in Table 3.

4.2 Comparison of optical and CO redshifts

In general, CO lines provide excellent systemic redshifts for galaxies, by tracing the extended molecular gas distribution rather than the ionised gas produced by shocked outflows or accretion onto an AGN. The latter is typically traced by high-ionisation, e.g. broad $\text{CIV}\lambda 1549$ lines, which have been shown to be systematically blue-shifted with respect to the systemic redshift in quasars (e.g. Richards et al. 2002), and by the $\text{Ly}\alpha$ line, which in the majority of high-redshift CO detections is blue-shifted with respect to the CO redshift due to outflows and dust obscuration (e.g. Hainline et al. 2004). The purpose of this section is to determine if similar systematic offsets between the CO and $\text{Ly}\alpha$ redshifts exist within the SMG population. We have measurements of the $\text{Ly}\alpha$ redshifts for eight of the CO-detected SMGs, see Table 2.

A large fraction of CO line profiles shown in Fig. 1 are double peaked or asymmetric, making it difficult to accurately determine the CO redshift by fitting Gaussian profiles to the spectra. Instead, the CO redshift of a source was determined by computing its flux-weighted redshift, i.e. $z_{\text{CO}} = \sum I(z)z / \sum I(z)$. The error on the redshift is given by $\Delta z_{\text{CO}}^2 = \sum I(z)(z - z_{\text{CO}})^2 / \sum I(z)$. The CO redshifts computed in this way are listed in Table 2.

In Fig. 3 we have plotted the distribution of velocity offsets corresponding to the differences between the CO and $\text{Ly}\alpha$ redshifts for the SMG sample. Negative velocity-offsets correspond to blue-shifted UV emission with respect to the systemic CO redshift. Also shown are the velocity offsets for the four SMGs with $\text{H}\alpha$ redshifts.

The velocity offsets between the $\text{Ly}\alpha$ and CO redshifts of

SMGs show a tendency for blue-shifted offsets (five and two SMGs have blue- and red-shifted offsets, respectively, with one source consistent with no velocity offset within the errors, $\sim 150 \text{ km s}^{-1}$), although this needs to be confirmed once a larger sample of SMGs is studied. The 15 QSOs detected in CO to date show a similar tentative excess of negative CO- $\text{Ly}\alpha$ velocity offsets (Fig. 3), although in this case the shift is due to strong absorption of the line – most likely from gas on small scales near the nucleus. In the case of SMGs, the offsets are likely to come from absorption from a wind on larger kpc-scales – where we only see the line scattered from the far side of the wind/shell due to the absorption of the blueshifted component.

It is clear from Fig. 3 that in the majority of the SMGs, significant velocity offsets exist between the $\text{Ly}\alpha$ and CO emission. Such large offsets illustrate how easy it would be to miss a CO line based on blind tuning to the restframe-UV redshift, and highlight the need for future submm/mm correlators with large instantaneous bandwidths.

Realising the potential danger of not detecting some of the SMGs because of large offsets between the CO and restframe-UV redshifts, we have undertaken a programme to target SMGs using the near-infrared spectrographs NIRSPEC on Keck-II, OHS on Subaru and ISAAC on the VLT, to allow us to measure redshifts from restframe optical emission lines, which should provide more reliable estimates of the systemic redshifts (e.g. Simpson et al. 2004; Swinbank et al. 2004). The usefulness of this approach is demonstrated by the hashed histogram in Fig. 3 which shows that for the four SMGs with redshifts derived from $\text{H}\alpha$ (or $[\text{OII}]\lambda 3727 \text{ \AA}$ in the case of SMM J02396–0134 – Soucail et al. 1999), the velocity offsets amount to no more than $\pm 75 \text{ km s}^{-1}$.

4.3 CO Luminosities and gas masses

The CO line luminosities, L'_{CO} , of the individual SMGs were derived from their velocity-integrated line flux densities following Solomon et al. (1997), and corrected for gravitational lensing if necessary (see Table 3). For the eight sources detected in CO(3–2) we find a median luminosity of $\langle L'_{\text{CO}(3-2)} \rangle = (3.8 \pm 2.3) \times 10^{10} \text{ K km s}^{-1} \text{ pc}^2$. Two sources were detected in CO(4–3) (SMM J09431+4700 and SMM J13120+4242) and two in CO(2–1) (SMM J02399–0134 and ERO J16450+4626). Note that for HR 10/ERO J16450+4626 we have used the CO(2–1) spectrum (Andreani et al. 2000) rather than the CO(1–0) measurement by Greve et al. (2003) which lacks velocity information.

Assuming intrinsic velocity/area-averaged brightness temperature line ratios corresponding to an optically thick, thermalised gas, i.e. $r_{32} = T_b(3-2)/T_b(1-0) = L'(3-2)/L'(1-0) = 1$, and similarly $r_{43} = 1$ and $r_{21} = 1$, we derive a median CO(1–0) luminosity of $\langle L'_{\text{CO}(1-0)} \rangle = (3.8 \pm 2.0) \times 10^{10} \text{ K km s}^{-1} \text{ pc}^2$, where we have included all sources, except for the non-detections. If we assume more realistic values of $r_{32} = 0.64$ (Devereux et al. 1994), $r_{43} = 0.45$ (Papadopoulos et al. 2000), and $r_{21} = 0.9$ (e.g. Braine & Combes 1992; Aalto et al. 1995) as derived from ISM studies in local starburst galaxies, we instead find a median CO(1–0) luminosity of $\langle L'_{\text{CO}(1-0)} \rangle = (5.9 \pm 3.6) \times 10^{10} \text{ K km s}^{-1} \text{ pc}^2$.

The observed CO luminosities are converted into molecular gas masses using $M(\text{H}_2) = X_{\text{CO}} L'_{\text{CO}(1-0)}$, where $X_{\text{CO}} = 0.8 (\text{K km s}^{-1} \text{ pc}^2)^{-1} M_{\odot}$ is the conversion factor appropriate for UV-intense environments, as derived from observations of local ULIRGs (Downes & Solomon 1998). The molecular gas masses derived for each source are given in Table 3 for assumed

(2–1)/(1–0), (3–2)/(1–0) and (4–3)/(1–0) line ratios of unity. The distribution of SMG molecular gas masses is shown in Fig. 4, from which we derive a median value $\langle M(\text{H}_2) \rangle = (3.0 \pm 1.6) \times 10^{10} M_\odot$ (not including the upper limits from the non-detections). Given the modest size of our sample we are not in a position to separate the observed scatter in the distribution of molecular gas masses into components due to varying inclination angles, differences in excitation conditions, and underlying scatter in the mass distribution of SMGs.

Since these molecular gas mass estimates are based on observations of high- J CO transitions with $J \geq 2$ and made assuming a thermalised, optically thick gas, it is possible that significant amounts of cold, possibly sub-thermal, molecular gas, could be present, but only detectable in lower CO transitions (e.g. Papadopoulos et al. 2001; Papadopoulos & Ivison 2002; Greve et al. 2003). Furthermore, if metal-poor gas is present, the gas mass could be higher. Finally, CO is primarily a tracer of material in the diffuse ISM and it is possible that a significant amount of dense and clumpy gas ($\gtrsim 10^4 \text{ cm}^{-3}$) is missed by our observations (e.g. Carilli et al. 2004). The quoted H_2 masses in Table 3 should therefore be considered as lower limits to the total amount of molecular gas.

Our estimates of the molecular gas mass include a non-negligible fraction of Helium which is accounted for in the adopted value of the conversion factor (Downes & Solomon 1998). The amount of neutral gas (HI), however, is particularly difficult to determine and significant uncertainty is associated with $M(\text{HI})$ -estimates at high redshift (e.g. De Breuck et al. 2003a). Estimates of the H_2 -to-HI mass ratio in infrared-luminous *IRAS* galaxies range from ~ 0.5 in systems with $L_{\text{FIR}} \sim 10^{10-11} L_\odot$ (Andreani et al. 1995) to ~ 4 for $L_{\text{FIR}} \sim 10^{12} L_\odot$ systems (Mirabel & Sanders 1989). The latter value may apply to the extremely far-infrared luminous SMGs. However, most of the neutral gas in local galaxies is on very large scales ($\gtrsim 10 \text{ kpc}$) and thus may not be relevant for our estimates.

Finally, we have looked for evidence of a correlation between molecular gas content and redshift. Such a trend would be indicative of evolution within the redshift range spanned by the SMG population. If we only consider the 13 sources observed in CO as part of our statistically-complete survey (i.e. not including SMM J02396–0134) and split the sample into low- and high-redshift halves at the median redshift of the sample, $\langle z \rangle = 2.4$, we find that the CO detection rate in the high-redshift ($z \geq 2.4$) subset is 5/7 (71 per cent) compared to just 2/6 (33 per cent) for sources at $z < 2.4$. The higher detection rate at $z \gtrsim 2.4$ could be indicative of evolution over the redshift range $z \sim 1-3$ in the gas masses associated with the most luminous starbursts. Using a Cox/Hazard survival analysis, we find that the formal likelihood of a variation in detection rate with redshift in the 13 sources observed by our survey is $P = 0.995$, suggestive of a real trend. If we instead include all the sources listed in Table 2 the trend weakens (the detection rates become 4/8 and 8/10 for the low- and high-redshift bins, respectively). This is unsurprising since the bias against publishing non-detections in the literature means that this comparison is less reliable than that for our statistically-complete sample.

4.4 Line widths and dynamical masses

A striking feature of the SMG population is their typically broad CO line profiles, Table 3. The median observed FWHM of the sample is $780 \pm 320 \text{ km s}^{-1}$ and the median FWZI is 850 km s^{-1} . These values do not take into account any geometrical effects, such as inclination angle, which could effect the individual estimated

line widths by more than a factor of two. For example, in the case of SMM J14011+0252 it is plausible that the relatively small line width is due to the fact that the angular momentum vector of the system is closely aligned to our line-of-sight (Tecza et al. 2004). Hence the observed FWHM are firm lower-limits to the true orbital velocities and assuming our sample has random orbital inclinations, then the average correction should be $\sec \pi/4 = 1.4\times$.

In order to use our observed CO line widths to derive the dynamical mass of the SMGs we must know the spatial extent of the CO. However, so far CO emission has been reliably resolved in only one SMG: SMM J02399–0136 (Genzel et al. 2003). While a number of SMGs show tentative evidence of extended CO emission (Ivison et al. 2001; Neri et al. 2003; Greve et al. 2003), their low signal-to-noise ratios prevent a robust determinations of the source size. Instead, we have assumed a conservative source diameter of $\sim 0.5''$, which corresponds to a median linear diameter of 3.7 kpc (correcting for gravitational lensing where relevant), see Table 3. This is a factor of two smaller than the source sizes estimated by Neri et al. (2003), but consistent with characteristic size estimates from recent high-resolution radio observations of SMGs with MERLIN by Chapman et al. (2004), and with results from high-resolution PdBI CO observations (Tacconi et al. 2005) of the three SMGs detected in CO by Neri et al. (2003).

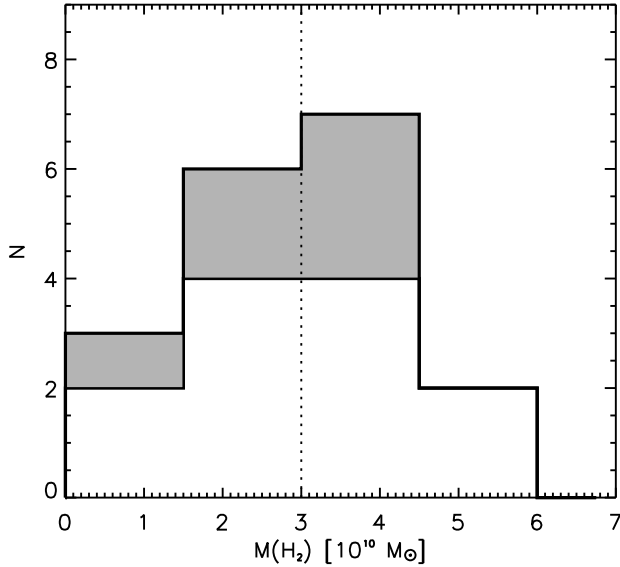
Another notable feature of our sample is the high fraction of SMGs which show evidence of double-peaked CO line profiles. Four sources (SMM J02396–0134, SMM J02399–0136, SMM J16359+6612 and SMM J16366+4105) show unambiguous double-peaked profiles, and a further two sources (SMM J04431+0210 and SMM J16368+4057) are better fit by a double Gaussian than a single Gaussian, as measured by the reduced χ^2 of the fit. In the case of SMM J16368+4057 further evidence of multiple CO peaks comes from H α IFU observations (Swinbank et al. in preparation) which show emission components at velocity-offsets similar to those we infer from the double Gaussian fit. Thus, at least 4/12 (33 per cent), and possibly as many as 6/12 (50 per cent), of the detected sample show evidence of having more than one CO-emitting component in their spectra. Comparing the occurrence of double-peaked line profiles in sources as a function of redshift within our sample, we see that the double-peaked sources appear to lie at the lower-redshift end of our sample, 5/7 at $z \leq 2.5$, compared to 1/5 for the SMGs at $z > 2.5$. A possible explanation for this tentative trend is discussed later.

Such multi-peaked line profiles are a tell-tale sign of orbital motion under the influence of gravity, and can usually be attributed to either a disk or a merger. To determine the likely structure of the gas reservoir, we use our median gas mass ($3 \times 10^{10} M_\odot$) and adopt a typical diameter of $\sim 4 \text{ kpc}$ for the gas reservoir, to derive a mass surface density of ($\Sigma \sim 2.4 \times 10^3 M_\odot \text{ pc}^{-2}$) for this structure. This is extremely high and implies that if the gas is present in a disk then this will have a Toomre parameter $Q < 1^2$, indicating it will be unstable to bar formation. The disk would then collapse on a timescale comparable to the sound crossing time, which is much shorter than the expected $\sim 10-100 \text{ Myr}$ duration of the SMG phase, see §5.4. We conclude that the kinematics responsible for the double-peaked CO lines are unlikely to arise from gas

² Toomre's stability criterion says that $Q = \frac{2v_s\Omega}{\pi G\Sigma} \geq 1$ in order for a gaseous disk to be stable: see e.g. Binney & Tremaine (1987). For a surface density $\Sigma \sim 2.4 \times 10^3 M_\odot \text{ pc}^{-2}$, Q will always be less than one for any realistic values of the sound speed v_s and circular frequency Ω .

Table 3. Physical properties derived from the CO observations.

Source	μ_L^a	$D(1'')^b$ (kpc)	Transition	$L'_{CO}{}^b$ ($\times 10^{10} \text{ K km s}^{-1} \text{ pc}^2$)	$M(\text{H}_2)^{b,c}$ ($\times 10^{10} M_\odot$)	ΔV_{FWHM}^d (km s^{-1})	M_{dyn}^e ($\times 10^{11} M_\odot$)
SMM J02396–0134	2.5	3.3	(2–1)	2.1 ± 0.2	1.7 ± 0.2	780 ± 60	1.2
SMM J02399–0136	2.5	3.2	(3–2)	4.8 ± 0.8	3.8 ± 0.6	1360 ± 50	3.5
SMM J04431+0210	4.4	1.9	(3–2)	1.1 ± 0.2	0.9 ± 0.2	350 ± 60	0.1
SMM J09431+4700	1.2	6.3	(4–3)	2.7 ± 0.3	2.2 ± 0.2	420 ± 50	0.7
SMM J10523+5722	1.0	8.1	(3–2)	≤ 2.1	≤ 1.4
SMM J10524+5724	1.0	7.8	(3–2)	≤ 4.6	≤ 3.0
SMM J12360+6210	1.0	8.5	(3–2)	≤ 2.9	≤ 1.6
SMM J13120+4242	1.0	7.5	(4–3)	5.3 ± 0.9	4.2 ± 0.7	530 ± 50	1.2
SMM J13123+4239	1.0	8.3	(3–2)	≤ 4.1	≤ 2.4
SMM J14011+0252 ^f	5.0	1.6	(3–2)	1.9 ± 0.2	1.5 ± 0.2	190 ± 11	0.03
SMM J16368+4057	1.0	8.3	(3–2)	7.0 ± 0.6	5.6 ± 0.5	840 ± 110	3.5
SMM J16359+6612	22	0.4	(3–2)	0.4 ± 0.2	0.3 ± 0.2	500 ± 100	0.06
SMM J16363+4055	1.0	8.3	(3–2)	≤ 1.7	≤ 0.9
SMM J16363+4056	1.0	8.5	(2–1)	≤ 4.1	≤ 1.8
SMM J16366+4105	1.0	8.2	(3–2)	5.7 ± 1.0	4.6 ± 0.7	870 ± 80	3.7
SMM J16371+4053	1.0	8.3	(3–2)	3.0 ± 0.9	2.4 ± 0.7	830 ± 130	3.4
ERO J16450+4626	1.0	8.5	(2–1)	3.8 ± 0.3	3.0 ± 0.2	400 ± 20	0.8
SMM J22174+0015	1.0	7.8	(3–2)	3.8 ± 1.0	3.0 ± 0.7	780 ± 100	2.8
Median ^g		7.5 ± 3.1		3.8 ± 2.0	3.0 ± 1.6	780 ± 320	1.2 ± 1.5

^a Assuming equal flux magnification and linear magnification.^b $D(1'')$ is the linear distance in kpc corresponding to $1''$ at the given redshift and corrected for the lensing amplification μ_L .^c Derived assuming $X_{\text{CO}} = 0.8 (\text{K km s}^{-1} \text{ pc}^2)^{-1} M_\odot$.^d The line widths are derived from a single Gaussian fit to the line profile.^e Calculated adopting a source diameter of $0.5''$.^f The amplification factor for this source was recently revised from 2.5 to ~ 5 (see discussion in Swinbank et al. 2004).^g The non-detections (upper limits) are not included in the median.**Figure 4.** The distributions of molecular gas masses of the SMG sample assuming a conversion factor of $X_{\text{CO}} = 0.8 (\text{K km s}^{-1} \text{ pc}^2)^{-1} M_\odot$ and line ratios $r_{32} = r_{43} = 1$. Non-detections are included as the shaded part of the histogram. The median gas mass of the sample, not including the non-detections, is $\langle M(\text{H}_2) \rangle = (3.0 \pm 1.6) \times 10^{10} M_\odot$ (dotted vertical line).

distributed in a stable disk, instead a more likely scenario is that they reflect a merger of two gas-rich components or from a disk collapsing under gravitational instability.

With almost all of the SMGs being spatially unresolved in CO we are unable to determine whether SMGs typically contain gaseous disks in their centres or if they are mergers. However, given their large gas mass densities, as well as the high fraction of double-peaked profiles we feel that SMGs are more likely to be mergers.

Additional evidence for a merger origin comes from the detection of close companions in CO in some of our fields (Neri et al. 2003), as these are likely to be interacting or merging given the small spatial and velocity differences. Thus, dynamical masses were calculated using the ‘merger’ formula given in Neri et al. 2003 (see also Genzel et al. 2003), and reported in Table 3. Neri et al. (2003) assumed a stable disk model which gives dynamical masses lower by a factor of two; but since they adopted a characteristic source sizes twice as large as ours, the resulting dynamical mass estimates coincide. The median SMG dynamical mass within $R \lesssim 2 \text{ kpc}$ is $\langle M_{\text{dyn}} \rangle \simeq (1.2 \pm 1.5) \times 10^{11} M_\odot$, where we have applied an average correction of $1.4\times$, assuming random inclinations for the sample overall. We estimate a median molecular gas-to-dynamical mass fraction in SMGs of $\langle M_{\text{gas}}/M_{\text{dyn}} \rangle \sim 0.3$ (~ 0.5 if we assume a disk model). This indicates that the contribution of the gas reservoir to the dynamics of the central regions of typical SMGs is substantial, and that the gas has already concentrated into the central regions of the galaxy by some dissipative process. It should be noted, however, that significant uncertainties are associated with the dynamical mass estimates, especially if the system is not in dynamical equilibrium, or if the observed line is not a good tracer of the dynamical state of the galaxy (also see the discussion in Neri et al. 2003).

5 COMPARISON WITH OTHER POPULATIONS

Unlike optical/near-infrared and X-ray observations, CO observations are relatively unaffected by either dust extinction or AGN activity, and a comparison between the CO properties of SMGs and that of other galaxy populations could therefore potentially provide us with a clean way of comparing the bulk properties of SMGs with other galaxy populations at both high and low redshifts; although, by virtue of the submm selection technique such a comparison is of course biased towards dust-enshrouded sources.

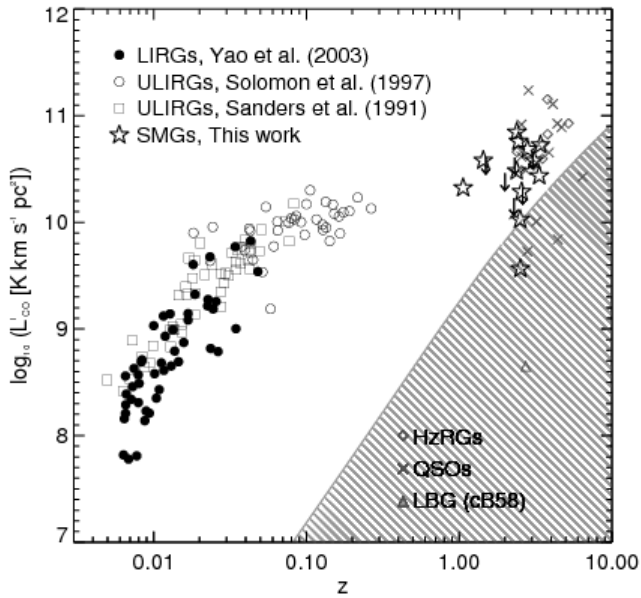


Figure 5. The relationship of $\log_{10}(L'_{\text{CO}})$ with redshift for the (U)LIRGs samples of Sanders et al. (1991), Solomon et al. (1997), and Yao et al. (2003), and for the sample of high-redshift (sub)mm-selected sources presented in this paper. The CO luminosities have been corrected for gravitational amplification where necessary. Also shown are the (lensing-corrected) CO luminosities for HzRGs, QSOs and LBGs listed in Table 4, with the exception of Q 0957+561 and MG 0414+0534 which have unknown gravitational magnification factors. The CO luminosities for the (U)LIRGs are all based on the CO(1–0) line, whereas the luminosities of the high-redshift sources are entirely derived from CO $J = J + 1 \rightarrow J$ transitions with $J + 1 \geq 2$ (Table 4). Upper limits on the CO luminosities for the 7 SMGs not detected in CO are represented by downward pointing arrows. The hashed area denotes the region where sources are precluded from detection due to an integrated CO(3 – 2) flux limit of $I_{\text{CO}} = 0.3 \text{ Jy km s}^{-1}$. Of our sample, only SMM J16359+6612 with its very large amplification factor ($\mu = 22$) is detectable below this limit.

We list in Table 4 *all* non-SMG CO sources detected at $z \geq 1$. The bulk of these are extreme AGN such as submm-bright, high-redshift radio galaxies (HzRGs) or QSOs (e.g. Omont et al. 1996; Papadopoulos et al. 2000; Cox et al. 2002).

Due to their similar properties, in particular their large far-infrared luminosities, distorted morphologies and optical/near-infrared colours (e.g. Ivison et al. 2002; Smail et al. 2004), SMGs are commonly thought to be high-redshift analogues of local ULIRGs. To test this claim we now compare the CO properties of SMGs with ULIRGs. To this end we have used the samples of Sanders et al. (1991; SA91) and Solomon et al. (1997; SO97) which consist of 48 and 37 local ULIRGs (and less luminous LIRGs) in the redshift range $z = 0.03$ – 0.27 , respectively, and the sample of 60 (U)LIRGs from Yao et al. (2003; Y03), selected from the SCUBA Local Universe Galaxy Survey (SLUGS, Dunne et al. 2000).

5.1 CO luminosities and gas masses

In Fig. 5 we plot the CO luminosities of the SMG sample as a function of redshift along with the CO(1–0) luminosities of the (U)LIRG samples of SA91, SO97, and Y03. From Fig. 5 it is

clear that while the most luminous ULIRGs have CO luminosities comparable to those of the faintest detected SMGs, SMGs are generally more CO luminous than the local (U)LIRGs. In §4.3 we found the median CO line luminosity of the SMG sample to be $\langle L'_{\text{CO}} \rangle = (3.8 \pm 2.0) \times 10^{10} \text{ K km s}^{-1} \text{ pc}^2$, which is almost a factor of four greater than the average CO luminosity of the ULIRGs from SO97. Furthermore, while the CO luminosities of the (U)LIRGs are all based on the lowest and least excitation-biased CO(1–0) rotational line, all of the SMGs are detected in higher transitions. Hence, the CO luminosities based on the high- J lines for SMGs should be regarded as lower limits on the CO(1–0) luminosities, unless the lines are fully thermalised at high temperatures and optically thick.

The (U)LIRGs lie on a well-defined locus in Fig. 5, which is extended to the highest redshifts and CO luminosities by the SMG sample. The lower boundary of this trend is determined by the sensitivity limits of the CO observations, while the upper bound is a real astrophysical limit. The steady decline in the CO luminosity of SMGs to ULIRGs and LIRGs seen in Fig. 5 is likely to reflect the evolution in the molecular gas-content of the most luminous starburst galaxies as a function of redshift, despite the expected increasing mass of a typical galaxy with cosmic time. A possible caveat is the assumption of a constant conversion factor in (U)LIRGs and SMGs. In (U)LIRGs the X_{CO} conversion factor is about 4.5 times lower than in normal spiral galaxies, and it is possible that for the yet more luminous SMGs it is even lower.

Also shown in Fig. 5 are the CO luminosities of all HzRGs and QSOs detected to date (Table 4), as well as the only optically-selected Lyman break galaxy (LBG), MS 1512–cB58 ($z = 2.73$), detected in CO (Baker et al. 2004). Their large apparent scatter is due to many of these objects being gravitationally-lensed, increasing the effective sensitivity limits of their observations beyond the capabilities of current instruments in blank fields. SMGs are seen to have CO luminosities comparable to the most luminous HzRGs (e.g. Papadopoulos et al. 2000; De Breuck et al. 2003a, 2003b) and QSOs (e.g. Carilli et al. 2002a; Walter et al. 2003). In contrast, the CO luminosity of the typical-luminosity LBG cB58, $4.2 \times 10^9 \text{ K km s}^{-1} \text{ pc}^2$, is nearly two orders of magnitude ($\sim 90\times$) less than the median value for SMGs, despite its similar redshift. With only one LBG detected in CO so far it is not possible to make any meaningful conclusions about the molecular gas content of this population, except that the low CO luminosity of cB58 compared to that of SMGs is consistent with the faintness of LBGs at submm wavelengths and their relatively low (compared to SMGs) star-formation rates as inferred from optical spectroscopy (Blain et al. 1999; Adelberger & Steidel 2000).

5.2 CO line widths and dynamical masses

In §4.4 we found that $\gtrsim 33$ per cent of the CO-detected SMGs have double-peaked CO profiles. This is comparable to the fraction of double-peaked CO spectra in local ULIRGs (SO97). The median FWHM CO linewidth for the SMG sample is $780 \pm 320 \text{ km s}^{-1}$, about 3 and 4 times larger than the averages for the SA91 and SO97 ULIRG samples, respectively. Since the dynamical mass depends on the square of the velocity dispersion ($M_{\text{dyn}} \sim R\sigma^2$), this would naively suggest that the dynamical masses of the SMGs are ~ 9 – 16 times larger than that of ULIRGs (if the gas kinematics sample similar radii in the galaxies). From detailed interferometric studies of the circumnuclear gas in local ULIRGs Downes & Solomon (1998) find a median dynamical mass of $\sim 6 \times 10^9 M_{\odot}$ within $R \lesssim 0.6 \text{ kpc}$ – about $20\times$ smaller than the mass enclosed within

Table 4. List of published high-redshift CO detections of LBGs, QSOs and HzRGs. The sources are sorted according to their redshifts. This table, together with Table 2 summarises the complete list of CO detections of sources at $z \geq 1$ to date. The velocity-integrated line fluxes, I_{CO} , have not been corrected for gravitational amplification.

Source	Type	Transition	z_{spec}	z_{CO}	ΔV_{FWHM} (km s^{-1})	I_{CO} (Jy km s^{-1})	Ref.
MS 1512–cB 58 ^a	LBG	(3–2)	2.727	2.7265 \pm 0.0004	174 \pm 43	0.37 \pm 0.08	[1]
Q 0957+561 ^a	QSO	(2–1)	1.413	1.414	440	1.2	[2],[3]
IRAS F10214+4724 ^a	QSO	(3–2)	2.286	2.2867 \pm 0.0003	250	21	[4],[5]
		(3–2)	...	2.2855 \pm 0.0003	230 \pm 30	4.1 \pm 0.9	[6]
		(3–2)	...	2.2854 \pm 0.0001	220 \pm 30	4.2 \pm 0.8	[7]
		(6–5)	...	2.2857 \pm 0.0003	240 \pm 30	9.4 \pm 2.0	[6]
H 1413+117 ^a	QSO	(3–2)	2.5582 \pm 0.0003	2.558	326	8.1	[8]
		(3–2)	352 \pm 81	14.4 \pm 4.4	[9]
		(3–2)	...	2.5579	362 \pm 23	9.9 \pm 0.6	[10]
		(3–2)	...	2.55784 \pm 0.00003	416 \pm 6	13.2 \pm 0.2	[11]
		(4–3)	...	2.5579	375 \pm 16	21.1 \pm 0.8	[10]
		(5–4)	...	2.5579	398 \pm 25	24.0 \pm 1.4	[10]
		(7–6)	...	2.5579	376	47.3 \pm 2.2	[10]
VCV J1409+5628	QSO	(3–2)	2.562	2.585 \pm 0.001	370 \pm 60	2.4 \pm 0.7	[12]
		(3–2)	...	2.5832 \pm 0.0001	311 \pm 28	2.3 \pm 0.2	[13]
		(7–6)	4.1 \pm 1.0	[13]
MG 0414+0534 ^a	QSO	(3–2)	2.639 \pm 0.002	2.639	580	2.6	[14]
LBQS 1230+1627B	QSO	(3–2)	2.735 \pm 0.005	2.741 \pm 0.002	...	0.80 \pm 0.26	[15]
RX J0911+0551 ^a	QSO	(3–2)	2.800	2.796 \pm 0.001	350 \pm 60	2.9 \pm 1.1	[12]
SMM J04135+1027 ^a	QSO	(3–2)	2.837 \pm 0.003	2.846 \pm 0.002	340 \pm 120	5.4 \pm 1.3	[12]
MG 0751+2716 ^a	QSO	(4–3)	3.200 \pm 0.001	3.200	390 \pm 38	5.96 \pm 0.45	[16]
APM 08279+5255 ^{a, b}	QSO	(1–0)	3.87	3.9	...	0.150 \pm 0.045	[17]
		(1–0)	0.22 \pm 0.05	[18]
		(2–1)	1.15 \pm 0.54	[17]
		(4–3)	...	3.9114 \pm 0.0003	480 \pm 35	3.7 \pm 0.5	[19]
		(9–8)	...	3.9109 \pm 0.0002	...	9.1 \pm 0.8	[19]
PSS J2322+1944 ^a	QSO	(1–0)	4.1108 \pm 0.0005	4.1192 \pm 0.0004	200 \pm 70	0.19 \pm 0.08	[20]
		(2–1)	0.92 \pm 0.03	[20]
		(4–3)	...	4.1199 \pm 0.0008	375 \pm 41	4.21 \pm 0.40	[21]
		(5–4)	...	4.1199 \pm 0.0008	273 \pm 50	3.74 \pm 0.56	[21]
BRI 1335–0417 ^b	QSO	(2–1)	4.398 \pm 0.028	4.4074 \pm 0.0015	420 \pm 60	0.44 \pm 0.08	[22]
		(5–4)	2.8 \pm 0.3	[23]
BRI 0952–0115 ^a	QSO	(5–4)	4.426 \pm 0.020	4.4337 \pm 0.0006	230 \pm 30	0.91 \pm 0.11	[15]
BRI 1202–0725 ^b	QSO	(2–1)	4.69	0.49 \pm 0.09	[22]
		(4–3)	280 \pm 30	1.5 \pm 0.3	[24]
		(5–4)	...	4.6932 \pm 0.002	320 \pm 35	2.40 \pm 0.30	[25]
		(5–4)	220 \pm 74	2.7 \pm 0.41	[25]
		(7–6)	...	4.6915 \pm 0.001	250 – 300	3.1 \pm 0.86	[24]
SDSS J1148+5251	QSO	(3–2)	6.43 \pm 0.05	6.418 \pm 0.004	320	0.18 \pm 0.04	[26]
		(6–5)	...	6.4187 \pm 0.0006	279	0.73 \pm 0.076	[27]
		(7–6)	...	6.4192 \pm 0.0009	279	0.64 \pm 0.088	[27]
53 W002	HzRG	(3–2)	2.390 \pm 0.004	2.394 \pm 0.001	540 \pm 100	1.5 \pm 0.2	[28]
		(3–2)	...	2.3927 \pm 0.0003	420 \pm 40	1.20 \pm 0.15	[29]
B3 J2330+3927 ^b	HzRG	(4–3)	3.087 \pm 0.004	3.094	500	1.3 \pm 0.3	[30]
TN J0121+1320	HzRG	(4–3)	3.516	3.520	700	1.2 \pm 0.4	[31]
6C 1909+722	HzRG	(4–3)	3.5356	3.532	530 \pm 70	1.62 \pm 0.30	[32]
4C 41.17 ^b	HzRG	(4–3)	3.79786 \pm 0.0024	3.7958 \pm 0.0008	1000 \pm 150	1.8 \pm 0.2	[33]
4C 60.07 ^b	HzRG	(1–0)	3.788	3.791	\geq 1000	0.24 \pm 0.03	[34]
		(4–3)	...	3.791	...	2.50 \pm 0.43	[32]
TN J0924–2201	HzRG	(1–0)	5.1989 \pm 0.0006	5.202 \pm 0.001	250 – 400	0.087 \pm 0.017	[35]
		(5–4)	200 – 300	1.19 \pm 0.27	[35]

^a The source is gravitationally lensed.^b The CO emission is resolved.

[1] Baker et al. (2004); [2] Planesas et al. (1999); [3] Krips et al. (2003); [4] Brown & Vanden Bout (1991); [5] Solomon et al. (1992a); [6] Solomon et al. (1992b); [7] Downes et al. (1995); [8] Barvainis et al. (1994); [9] Wilner et al. (1995); [10] Barvainis et al. (1997); [11] Weiss et al. (2003); [12] Hainline et al. (2004); [13] Beelen et al. (2004); [14] Barvainis et al. (1998); [15] Guilloteau et al. (1999); [16] Barvainis et al. (2002); [17] Papadopoulos et al. (2001); [18] Lewis et al. (2002); [19] Downes et al. (1999); [20] Carilli et al. (2002b); [21] Cox et al. (2002); [22] Carilli et al. (2002a); [23] Guilloteau et al. (1997); [24] Omont et al. (1996); [25] Ohta et al. (1996); [26] Walter et al. (2003); [27] Bertoldi et al. (2003); [28] Scoville et al. (1997); [29] Alloin et al. (2000); [30] De Breuck et al. (2003a); [31] De Breuck et al. (2003b); [32] Papadopoulos et al. (2000); [33] De Breuck et al. (2005); [34] Greve et al. (2004a); [35] Klammer et al. 2005.

$R \lesssim 2$ kpc in SMGs (see Table 3). Assuming an isothermal mass distribution, the SMGs will have dynamical masses within 0.6 kpc roughly $6\times$ that of local ULIRGs.

We now turn to the comparison between SMGs and other high-redshift galaxy populations. Fig. 6a compares the distribution of velocity dispersions of our SMG sample with that of all high-redshift QSOs and HzRGs detected in CO to date. While there is

a substantial overlap between the SMG and QSO distributions, the latter is seen to peak at somewhat lower velocity dispersions than SMGs and we note that all QSOs have $\log \sigma \leq 2.4$ (corresponding to $\text{FWHM} \leq 590 \text{ km s}^{-1}$). Also, no QSO detected in CO show evidence of a double peaked line profile (although a few are spatially resolved – Papadopoulos et al. 2001; Carilli et al. 2002a). A Kolmogorov-Smirnov test suggests that the two distributions are

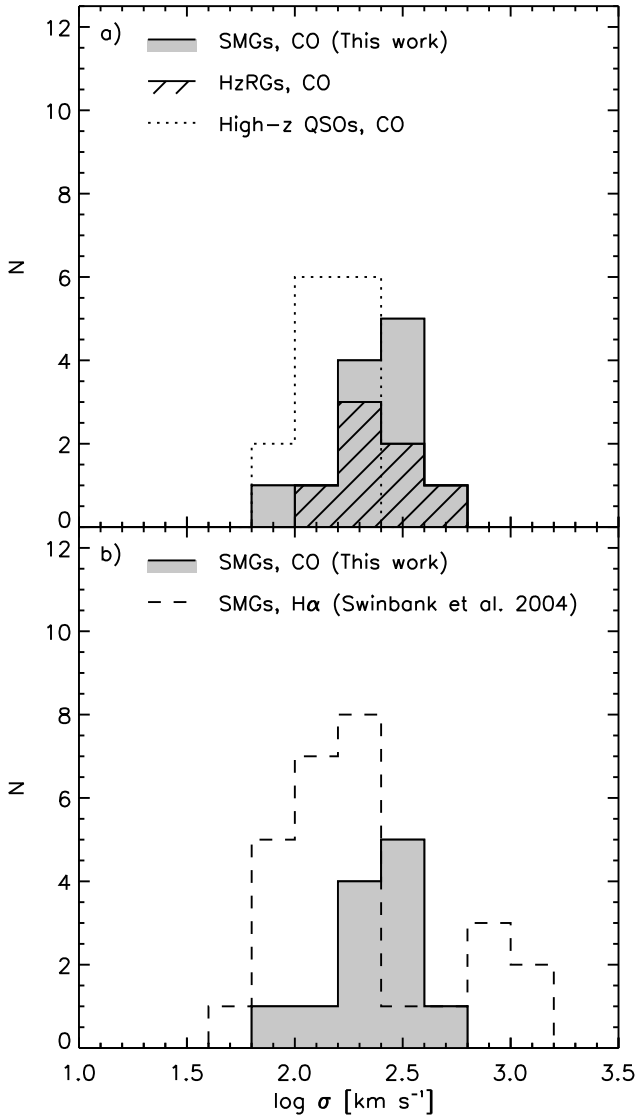


Figure 6. a) Distribution of CO velocity dispersions for high-redshift QSOs and HzRGs from Table 2 and our sample of CO-detected SMGs. In the cases of the two HzRGs 4C 60.07 and TN J0924–2201 we have adopted FWHM linewidths of 1000 and 325 km s^{−1}, respectively. In b), we compare with the measurements of the line widths of the H α line from near-infrared spectroscopy of a large sample of SMGs (Swinbank et al. 2004).

formally different at the 95 per cent confidence level. The apparently lower CO linewidths of QSOs is not clear, although it is possible that they are either intrinsically lower-mass systems or have smaller gas disks. In contrast, there is no discernable difference between the CO line widths of the SMGs and those HzRGs detected in CO. This suggests that the brightest SMGs have similar dynamical masses, and therefore possibly similar dark-matter halo masses, to HzRGs which are believed to be amongst the most massive objects in the high-redshift Universe (inferred from both the presence of a supermassive black hole and the strong clustering of HzRGs – e.g. Ford et al. 1994; Kooiman et al. 1995). However, such a conclusion is uncertain due to the small number of objects involved and will have to wait until a larger, more uniform sample of HzRGs has been observed in CO.

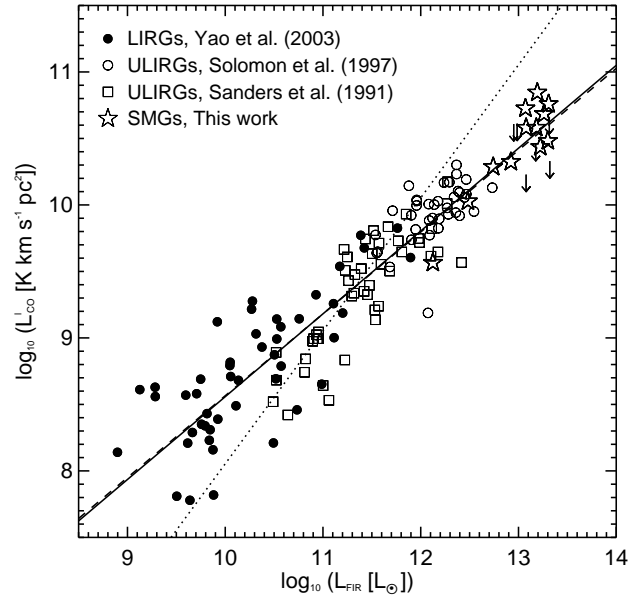


Figure 7. A comparison of the CO and far-infrared luminosities (L'_{CO} , L_{FIR}) for SMGs and local ULIRGs. As in Fig. 5 the arrows denote the 6 non-detections. The solid and dashed lines represent fits of the form $\log L'_{\text{CO}} = \alpha \log L_{\text{FIR}} + \beta$ to all three (U)LIRGs samples and to the combined (U)LIRGs and SMGs samples, respectively. The dotted line is the best fit to all four samples but where the slope has been fixed to unity.

In Fig. 6b we compare the CO line widths from our SMG sample with measurements of the width of the H α line from a recent near-infrared spectroscopic survey of 28 SMGs and high redshift, optically-faint, radio-selected starburst galaxies (OFRGs – see e.g. Chapman et al. 2005) by Swinbank et al. (2004). The two distributions span a similar range of velocity dispersions, but the CO sample is skewed towards higher values, resulting in a higher median value. We find that the average ratio between the CO and H α line widths for SMGs is $\langle \text{FWHM}_{\text{CO}} \rangle / \langle \text{FWHM}_{\text{H}\alpha} \rangle \sim 2$. The main reason for this is likely to be due to the CO tracing multiple components in the SMG whereas the long-slit H α spectroscopy is identifying only a single component due to the slit orientation or due to extreme obscuration in the second component. Part of the discrepancy may also reflect dust-obscuration within the galaxy providing only a partial view of the kinematics of the system, in contrast to the obscuration-independent measurement provided by CO. If this is the case, it could mean that the dynamical masses of SMGs are larger than suggested from their rest-frame optical spectra.

5.3 Star-formation efficiency and the $L'_{\text{CO}}-L_{\text{FIR}}$ relation

While the luminosity of the CO lines is an indicator of how much molecular gas a galaxy contains, it does not necessarily measure how efficiently this gas is being turned into stars. The star-formation efficiency (SFE) can be estimated from the ratio of the far-infrared luminosity of the system to the amount of molecular gas available to form stars, i.e. $\text{SFE} = L_{\text{FIR}} / M(\text{H}_2)$.

The far-infrared luminosities of the SMGs were estimated following Neri et al. (2003), $L_{\text{FIR}} = 1.9 \times 10^{12} S_{850}$, where L_{FIR} is in L_{\odot} and S_{850} in mJy. This assumes a modified grey-body model for the far-infrared emission with a dust temperature of

$T_d = 40$ K and emissivity $\propto \nu^{1.5}$. The median far-infrared luminosity of the SMG sample is $\langle L_{\text{FIR}} \rangle = (1.5 \pm 0.7) \times 10^{13} L_{\odot}$ which is nearly an order of magnitude larger than the most luminous local ULIRGs (Solomon et al. 1997). Assuming that the bulk of the far-infrared luminosity is powered by star-formation (Frayer et al. 1998; Alexander et al. 2005), we find a median star-formation efficiency of $\langle SFE \rangle = 450 \pm 170 L_{\odot} M_{\odot}^{-1}$ for the SMG sample, in agreement with the initial findings of Neri et al. (2003). This is somewhat higher than the typical starformation efficiency of the local ULIRGs studied by SO97 ($\langle SFE \rangle = 180 \pm 160 L_{\odot} M_{\odot}^{-1}$ – using a conversion factor of $X_{\text{CO}} = 0.8 (\text{K km s}^{-1} \text{pc}^2)^{-1} M_{\odot}$).

Perhaps a more straightforward measure of the star-formation efficiency is the continuum-to-line luminosity ratio, $L_{\text{FIR}}/L'_{\text{CO}}$, since it does not depend on X_{CO} . Locally, (U)LIRGs are observed to follow a scaling relation between L'_{CO} and L_{FIR} with the more far-infrared luminous galaxies having proportionally higher CO luminosities (Rickard & Harvey 1984; Young et al. 1984, 1986; Sanders & Mirabel 1985). In Fig. 7 we have plotted the SMGs onto the $L'_{\text{CO}} - L_{\text{FIR}}$ diagram along with the (U)LIRGs from our three low-redshift comparison samples. The SMGs extend the general trend seen for the local (U)LIRGs out to far-infrared luminosities $\gtrsim 10^{13} L_{\odot}$. A power-law fit to all three (U)LIRG samples yields $\log L'_{\text{CO}} = (0.62 \pm 0.09) \log L_{\text{FIR}} + (2.41 \pm 1.06)$. Including the SMGs in the fit yields $\log L'_{\text{CO}} = (0.62 \pm 0.08) \log L_{\text{FIR}} + (2.33 \pm 0.93)$, i.e. virtually no change in the fit at all. The combined SMG and local ULIRG samples have a statistically-significant correlation, as shown by a Spearman's rank-order correlation test, which yields a probability of $P < 0.0001$ that a random (uncorrelated) data set could result in the observed correlation coefficient ($r_S = 0.93$). From Fig. 7 there is even some evidence of a $L'_{\text{CO}} - L_{\text{FIR}}$ correlation within the SMG population itself (the probability of obtaining the observed correlation, $r_S = 0.70$, by chance is $P < 0.0142$). Moreover, the slope of the $L'_{\text{CO}} - L_{\text{FIR}}$ correlation inferred from the fit is significantly less than unity. This is clearly illustrated in Fig. 7 where the locus defined by the data points is seen to have a shallower slope than the line of equality.

The observed slope of the correlation in Fig. 7 implies that the $L_{\text{FIR}}/L'_{\text{CO}}$ ratio increases with L_{FIR} . Several studies have already shown that ULIRGs have higher $L_{\text{FIR}}/L'_{\text{CO}}$ ratios than the less luminous LIRGs, which in turn have higher ratios than spiral galaxies and GMCs (e.g. Sanders et al. 1986; Solomon & Sage 1988). This trend is shown in Fig. 8 where $L_{\text{FIR}}/L'_{\text{CO}}$ has been plotted as a function of redshift for the LIRG, ULIRG and SMG samples. The median $L_{\text{FIR}}/L'_{\text{CO}}$ ratios for LIRGs (Y03) and ULIRGs (SO97) are 50 ± 30 and $160 \pm 130 L_{\odot} (\text{K km s}^{-1} \text{pc}^2)^{-1}$, respectively. The median far-infrared to CO luminosity ratio for the SMGs is $360 \pm 140 L_{\odot} (\text{K km s}^{-1} \text{pc}^2)^{-1}$, which is about a factor of two higher than the median value for ULIRGs, and suggests that although some overlap exists between the two populations, in general SMGs have higher star-formation efficiencies, or a larger contribution to their far-infrared luminosities from a source other than star formation, e.g. an AGN. Although AGN are frequently found in SMGs using extremely deep X-ray observations, these observations also suggest that the AGN are bolometrically insignificant in the vast majority of SMGs (Alexander et al. 2003, 2005).

We underline that the above findings are strongly biased towards luminous SMGs, as they are based on a sample of predominantly bright SMGs. This selection effect in conjunction with the CO detection limit of our survey prevent us from probing the lower right portion of Fig. 8, where objects with low $L_{\text{FIR}}/L'_{\text{CO}}$ ratios reside. It is possible that such objects, which are found locally (see Fig. 8), will also be uncovered at high redshifts by fu-

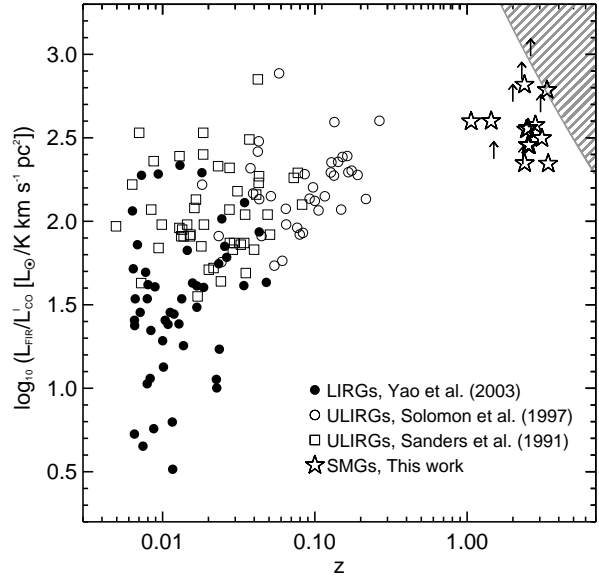


Figure 8. The star-formation efficiency as indicated by the observed ratio $L_{\text{FIR}}/L'_{\text{CO}}$ as a function of redshifts. Upward pointing arrows represent the 6 SMGs not detected in CO. The hashed region represents the no-detection zone for sources with integrated CO(3 – 2) fluxes of $I_{\text{CO}} \leq 0.3 \text{ Jy km s}^{-1}$ and submm fluxes of $S_{850\mu\text{m}} \leq 4 \text{ mJy}$.

ture deep submm and CO observations of a complete sample of high- z starburst galaxies. Intriguingly, however, the $L_{\text{FIR}}/L'_{\text{CO}}$ ratio of SMM J16359+6612, which has a far-infrared and CO luminosity comparable to the least luminous ULIRGs in the SO97 sample, is higher than almost all the sources in that sample ($360 L_{\odot} (\text{K km s}^{-1} \text{pc}^2)^{-1}$).

As a final check we repeated the above analysis using SMG far-infrared luminosities derived from their radio fluxes and using the radio-FIR correlation (Condon 1992; Yun, Reddy & Condon 2001). There is tentative evidence that this correlation applies out to high redshifts (Garrett 2002; Appleton et al. 2004), and arguably provides a more reliable estimate of the far-infrared luminosity than that based on the submm flux which has significant uncertainty associated with it due to the unknown dust properties of SMGs. The far-infrared luminosities derived using the radio information are generally larger, and the $L'_{\text{CO}} - L_{\text{FIR}}$ correlation therefore shallower ($\alpha = 0.59 \pm 0.08$). In this case, the SMG sample also exhibits a significant correlation, although this can partly be explained by the luminosity distance-squared stretching of the data points.

5.4 Discussion

In the previous three sub-sections it was found that SMGs have on average four times larger CO luminosities, 3–4 times larger line widths and a median $L_{\text{FIR}}/L'_{\text{CO}}$ ratio twice that of local ULIRGs. As argued in §4.4, the large line widths and molecular gas masses seen in SMGs are difficult to reconcile with a scenario in which the gas resides in a circumnuclear disk. This is in contrast to what is observed in local ULIRGs where the bulk of the gas is found in a $R \sim 0.5 \text{ kpc}$ disk or ring. In SMGs the gas is more likely to be distributed on scales of 2–3 kpc, as suggested by their radio morphologies (Chapman et al. 2004) as well as by high-resolution CO

observations of SMGs (Genzel et al. 2003; Tacconi et al. 2005). The typical gas-to-dynamical mass fraction in SMGs was estimated in §4.4 to be ~ 0.3 – almost two times higher than the median gas mass fraction in ULIRGs (~ 0.16 , Downes & Solomon 1998), assuming that the CO–H₂ conversion factor is the same for ULIRGs and SMGs. The local gas mass fraction in ULIRGs is measured within the molecular disk ($R \lesssim 0.5$ kpc) – but when averaged over scales of 2–3 kpc, which are the typical scales probed by our CO observations of SMGs, the gas fraction is likely to be significantly smaller. Although, we caution that some of the above arguments are based on a relatively small number of sources detected at low signal-to-noise or have non-negligible uncertainties associated with them (such as the CO conversion factor), they do seem to suggest, together with the generally higher far-infrared luminosities of SMGs, that the latter are neither high-redshift replicas of local ULIRGs, nor simply scaled-up versions. Rather SMGs appear to more gas-rich and more efficiently star-forming than local ULIRGs.

In this respect it is important to draw attention to observational studies of the depletion of molecular gas with starbursts in ULIRGs. In a sample of more than 50 (U)LIRGs, Gao et al. (1999) found a correlation between the CO(1–0) luminosity and the projected separation of the merging nuclei, which they took as evidence for molecular gas being rapidly depleted due to intense star formation as the merger progresses. If a similar picture applies at high redshift, the large CO luminosities and gas masses we find for SMGs would imply that these systems are extended, and caught in the early stages of merging. However, this might be a premature conclusion since Rigopoulou et al. (1999) did not find any evidence for a correlation between the gas mass and merger phase for local ULIRGs.

If the above trends are verified by future observations, it is interesting to speculate what physical mechanisms could be responsible for the differences between local ULIRGs and SMGs? Both populations appear to result from mergers and strong interactions (e.g. Sanders et al. 1991; Chapman et al. 2003c), so what makes the starbursts so much more efficient in SMGs? Numerical simulations have compared the gas flow in major mergers between two galaxies with strong bulges, and between two, gas-rich but bulge-less galaxies (Barnes & Hernquist 1996; Iono, Yun & Mihos 2004). In the first case, the gas forms shocked, dense filaments which dissipate energy and flow towards the centre where they form a nuclear ring which is stabilised by the gravitational potential of the bulge – slowing the rate of star formation. In the second scenario, the merger between two gas-rich but bulge-less galaxies, the gas forms an extended (~ 6 kpc), gravitationally-significant bar-like structure which allows the gas to funnel towards the centre. However, without the stabilising influence of the bulges in the progenitor galaxies, the gas cannot form a stable ring or disk and its density is further increased through the formation of bar-like structures, leading to a wide-spread and vigorous starburst.

These two theoretical scenarios suggest a structural difference between the progenitor galaxies may be at the heart of the differences in behaviour between ULIRGs and SMGs. The suggested structural differences are consistent with the expectations of the typical galaxies involved in mergers at low- and high-redshifts, with the former involving disk-galaxies with significant bulge components (e.g. Lilly et al. 1998), while the progenitor galaxies of SMGs at high redshift are much more likely to be gas-rich, disk-dominated systems with little or no bulge component (Wyse, Gilmore & Franx 1997; Ravindranath et al. 2004). If such structural differences between local and distant starbursts are real, the next question is: at what redshift does the transition occur? In §4.3

we found that SMGs at $z \sim 3$ have a higher CO detection rate than SMGs at $z \sim 2$ – consistent with the former being more gas-rich. Secondly, the slight preponderance, albeit tentative, of double-peaked CO line profiles at $z \sim 2$ is consistent with that of local ULIRGs and in contrast to SMGs at $z \sim 3$ (see §4.3 and §4.4). Although, these trends are tentative and need a larger survey to confirm or disprove them, together they may indicate a difference in the physical processes responsible for triggering intense star formation in massive galaxies at $z \sim 2$ compared to $z \sim 3$, with major mergers being responsible for much of this activity at lower redshifts (as is the case for local ULIRGs), but a separate mode (requiring less intense perturbations) capable of triggering similar bursts in the more gas-rich systems present at even higher redshifts.

In §5.3 we showed that luminous SMGs extend the $L_{\text{CO}} - L'_{\text{FIR}}$ relation of local ULIRGs to higher redshifts and luminosities, and accordingly have higher star-formation efficiencies than ULIRGs. Although, the star-formation efficiencies found for the SMGs could be severely overestimated if an AGN contributes significantly to the far-infrared luminosity, the detection of large amounts of molecular gas in SMGs along with recent X-ray (Alexander et al. 2003, 2005) and radio studies (Chapman et al. 2004) strongly suggest that the bulk of the far-infrared emission from SMGs is powered by a large-scale starburst and not from an AGN. While CO is a good indicator of the total metal-rich H₂ gas reservoir, it may be a worse indicator of the amount of dense gas present ($n \geq 10^5 \text{ cm}^{-3}$), that actually fuels star formation (Carilli et al. 2004). The latter could be particularly true in the tidally disrupted giant molecular clouds (GMCs) expected in ULIRGs, where a diffuse phase may dominate the CO emission but has little to do with star formation (Downes & Solomon 1998; Sakamoto et al. 1999). Such a diffuse phase could be even more pronounced in SMGs with their more extended distributions (Chapman et al. 2003c; Smail et al. 2004). This would explain why the $L_{\text{FIR}}/L'_{\text{CO}}$ ratio is found to be such a strong function of L_{FIR} , increasing for merging systems usually associated with the highest far-infrared luminosities. Interestingly, recent work shows that the SFE of dense gas, parametrised by the $L_{\text{FIR}}/L_{\text{HCN}(1-0)}$ ratio (the HCN $J = 1 - 0$ critical density is $2 \times 10^5 \text{ cm}^{-3}$), remains constant from GMCs all the way to ULIRG system (Gao & Solomon 2003; Solomon et al. 2003; Carilli et al. 2004).

The median star-formation rate of the 18 SMGs is $\langle SFR \rangle \simeq 700 M_{\odot} \text{ yr}^{-1}$, where we have assumed a Salpeter IMF and a very conservative limit corresponding to the starburst contributing only 50 per cent of the far-infrared luminosity (see Omont et al. 2001, but c.f. Alexander et al. 2005). Our findings in §5.1 and §5.2 have shown that SMGs are massive galaxies with enough molecular gas in them to sustain such a large star-formation rate for $\tau_{\text{SMG}} \sim M(\text{H}_2)/SFR \sim 3 \times 10^{10} M_{\odot} / 700 M_{\odot} \text{ yr}^{-1} \sim 40 \text{ Myr}$. By the end of such a burst most of the stellar mass corresponding to that of a massive spheroid would be in place. A gas depletion timescale of $\tau_{\text{SMG}} \sim 40 \text{ Myr}$ is comparable to the typical starburst ages ($\sim 100\text{--}200 \text{ Myr}$) derived from photometric modeling of the broad band optical/near-infrared colours of SMGs (Smail et al. 2004), although we note that large uncertainties are associated with both methods. For example, the CO observations only probe the gas within the central 10 kpc, and as a result the neutral gas – which is likely to be distributed on larger scales – has not been included in our estimate of the gas consumption time scale. If the H I gas is brought in from $\gtrsim 10 \text{ kpc}$ radius at $\sim 200 \text{ km s}^{-1}$ it would reach the central regions in less than 50 Myrs, where it could help sustain the vigorous starformation. Furthermore, the above gas consump-

tion time scale assumes a continuous starburst until all the gas is used – an unlikely scenario since it ignores the negative feedback effects from new-born massive stars and supernovae. For example, one could imagine the starburst terminating prematurely if the gas is removed by starburst- and/or AGN-driven winds only to fall back onto the galaxy at a later stage to fuel a second starburst, thus making the true gas exhaustion time scale longer. The 40 Myr should therefore be considered a strict lower limit on the starburst phase of SMGs.

An alternative estimate of the duration of the SMG phase can be made from the recent findings by Page et al. (2004) that the 15 per cent of QSOs at $z \sim 2$ which show absorption in their X-ray spectrum are detectable in the submm. Since only 3 per cent of radio-identified SMGs are QSOs (Chapman et al. 2005) this means that SMGs would have a typical lifetime which is $\sim 0.15/0.03 = 5$ times longer than that of QSOs. Adopting a QSO lifetime of 40 Myr (Martini & Weinberg 2001) yields a SMG life expectancy of $\tau_{SMG} \sim 200$ Myr – again larger than the gas consumption time scale.

If we assume that a large fraction of the gas mass of SMGs is eventually converted into stars (perhaps through repeated cycles of expulsion, infall and star formation), what are the resulting stellar masses of the descendants? Clearly SMGs already contain (perhaps substantial) stellar populations (Smail et al. 2004), however the stellar masses for SMGs are difficult to estimate due to significant dust extinction and the resulting uncertainties from the degeneracies between dust reddening and age in evolutionary spectral synthesis models. The best estimates to date, based on *IRK* photometry of 96 SMG and optically-faint μ Jy radio galaxies (Smail et al. 2004), suggest typical stellar masses of $M_{stars} \simeq 3 \times 10^{10} M_{\odot}$. Thus, combining the gas and stellar mass estimates we find that on average SMGs have baryonic masses of $\gtrsim 6 \times 10^{10} M_{\odot}$, which is comparable to the masses of local early type L^* galaxies.

The discussion above suggests that SMGs are in fact the progenitors of massive spheroids in the present-day Universe and that the build-up of the stellar population occurs rapidly ($40 \lesssim \tau_{SMG} \lesssim 100$ Myr), consistent with the old homogeneous stellar populations of local ellipticals. Further evidence in support of this is a) the strong clustering claimed for SMGs (Blain et al. 2004b), and b) the fact that the rest-frame optical properties of SMGs match the bright end of the luminosity function of spheroidal galaxies in nearby clusters (Smail et al. 2004).

6 IMPLICATIONS FOR STRUCTURE-FORMATION MODELS

Semi-analytical models of galaxy formation and evolution (Cole et al. 1994; Kauffmann et al. 1999; Cole et al. 2000; Somerville et al. 2001) have enjoyed a fair degree of success in reproducing the properties of galaxies in the local Universe, e.g. the luminosity function, the distribution of colours and disk scale lengths of galaxies, the observed mix of morphologies and the Tully-Fisher relation (e.g. Kauffmann et al. 1999; Cole et al. 2000). However, the key observable with which to benchmark models of galaxy formation and evolution is the mass assembly of galaxies, and in particular the assembly of baryonic mass, as a function of redshift.

Genzel et al. (2003) pointed out that if the extremely large baryonic mass ($\gtrsim 10^{11} M_{\odot}$) of SMM J02399–0136 was representative of the bright SMG population, then the high surface density of such sources would imply that the abundance of very massive baryonic systems at high redshift was about an order of magnitude

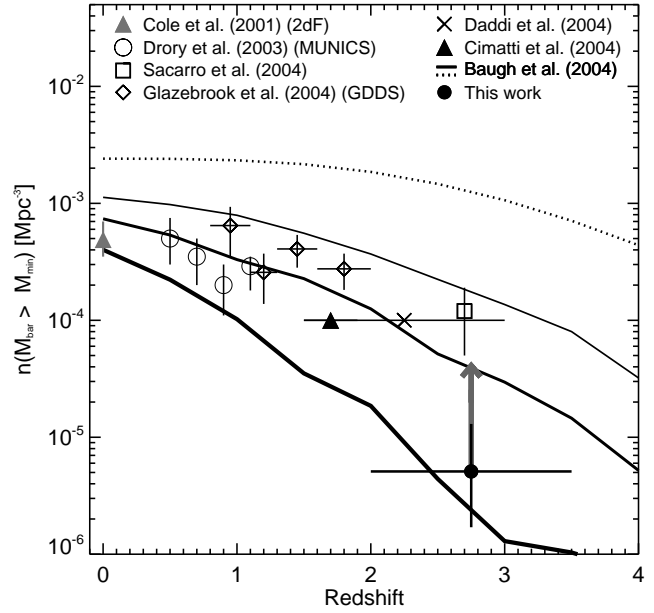


Figure 9. The co-moving number density of galaxies with baryonic masses $\sim 6 \times 10^{10} M_{\odot}$ as derived from CO observations of SMGs. The GAL-FORM model (Cole et al. 2001; Baugh et al. 2004) predictions of the abundances of galaxies with baryonic masses $\geq 5 \times$, $7 \times$, and $10 \times 10^{10} M_{\odot}$ as a function of redshift are shown as thin, medium and thick solid lines, respectively. The dotted curve represents the total baryonic matter content available in $\geq 10^{11} M_{\odot}$ dark matter halos, and is obtained by scaling the abundance of halos with the cosmological baryon-to-dark matter density ($\Omega_b/\Omega_{DM} = 0.13$). This provides a strict upper limit on the number density of massive baryonic galaxies at a given redshift. The observations can be reconciled within the CDM framework, provided that ~ 10 per cent of all baryons within dark matter halos are rapidly assembled into galaxies.

larger than predicted by semi-analytical models (see also Tecza et al. 2004).

Here we repeat this analysis using the 10 SMGs in our sample which lie in the redshift range $z = 2-3.5$ and have reliable gas mass estimates, to put lower limits on the co-moving number density of massive galaxies at high redshifts. The redshift interval considered translates into ~ 1.5 Gyr in terms of elapsed cosmic time, and corresponds to a co-moving volume of $1.8 \times 10^7 \text{ Mpc}^3$ per square degree. The average submm flux of the 10 SMGs is $\langle S_{850\mu\text{m}} \rangle = 8 \pm 4 \text{ mJy}$. The surface density on the sky of SMGs with fluxes $\gtrsim 8 \text{ mJy}$ is $285^{+231}_{-149} \text{ deg}^{-2}$ (Borys et al. 2003). Taking into account that a) about 60 per cent of the bright SMG population lie within $z = 2-3.5$ (Chapman et al. 2003b, Chapman et al. 2005), and b) the CO detection fraction of SMGs in the redshift range $2 \leq z \leq 3.5$ is 10/14 (~ 71 per cent), we estimate that the co-moving number density of galaxies with baryonic masses $\gtrsim 6 \times 10^{10} M_{\odot}$ in the redshift interval $z = 2-3.5$ is $\sim 5.1^{+7.6}_{-3.4} \times 10^{-6} \text{ Mpc}^{-3}$. The errors are estimated by propagating the 1- σ limits on the submm flux and number counts through the same calculation.

Since we only observe SMGs during their submm-luminous phase, we have to correct the derived space density by a factor corresponding to the ratio between the 1.5 Gyr which has elapsed over the redshift range $z = 2.0-3.5$ and the typical duration of the ‘SMG phase’. The latter is uncertain, but as we saw in §5.4 it is likely to lie in the range 40–200 Myr. Adopting 200 Myr as a

conservative upper value for the submm luminous phase, we estimate a correction factor of ~ 8 .

In Fig. 9 we have plotted our estimate of the co-moving number density of $\gtrsim 6 \times 10^{10} M_{\odot}$ systems at $z \sim 2.8$ and the (conservative) correction factor which must be applied. Our estimate of the abundances of massive galaxies at $z \sim 2.8$ is in good agreement with independent measurements at similar redshifts (Daddi et al. 2004; Saracco et al. 2004), and confirms the slow decline in the space density of massive galaxies as a function of redshift (Genzel et al. 2003; Glazebrook et al. 2004).

The abundance tracks of $\geq 5 \times 10^{10}$ and $\geq 7 \times 10^{10} M_{\odot}$ systems as predicted by the most recent GALFORM models (Cole et al. 2001; Baugh et al. 2004) are seen to envelope our estimated volume density. There are two reasons for the closer agreement between the observations and models than previous work: a) the typical baryonic mass of bright SMGs is not $2-3 m^*$ but rather $\sim 0.6 m^*$ and b) the new GALFORM model, which employs a top-heavy initial mass function (IMF) in order to account for the $850\text{-}\mu\text{m}$ number counts (Baugh et al. 2004), also predicts higher abundances of massive galaxies at high redshifts than previous models. Other semi-analytical models (Fontana et al. 2004; Granato et al. 2004) have also modified their recipes so that their models fit the data.

We stress, however, that by using a SMG timescale of 200 Myr, and not 40 Myr as suggested by the CO observations, our estimate of the correction factor is a conservative one. Furthermore, if the population of OFRGs, whose faint levels of submm flux is believed to be due their higher dust temperatures (Blain et al. 2004a; Chapman et al. 2005), have similar gas masses as classical SMGs (Swinbank et al. 2004; Smail et al. 2004), this would double our current estimate of the abundance of massive baryonic galaxies at high redshifts.

We conclude that given the small number of sources and crude redshift bins used in our calculations, and the large uncertainty on the correction factors which have to be applied, there is no evidence for a severe discrepancy between observations and the latest theoretical predictions. An increase in our sample size would not only allow us to confirm this but also allow us to split the sample into mass bins and compare with different mass track predictions.

7 CONCLUSIONS

We present results from a PdBI CO Survey of SMGs with radio counterparts. We successfully detect CO in 4 out of 10 SMGs observed, which brings the total number of SMGs detected by our survey to 7 out of 13 observed. In addition, we have also presented a detection of CO based on archival observations of SMMJ02396–0134. Combining these 14 sources with four CO-detected SMGs from the literature we have compiled a sample of 18 SMGs observed in CO of which 12 are detected. We use this unique sample to derive the bulk gas properties and masses of the most luminous SMGs.

- We find that the SMGs in our sample have a median CO luminosity of $\langle L'_{\text{CO}} \rangle = (3.8 \pm 2.0) \times 10^{10} \text{ K km s}^{-1} \text{ pc}^2$. This corresponds to a molecular gas mass of $\langle M(\text{H}_2) \rangle = (3.0 \pm 1.6) \times 10^{10} M_{\odot}$ (within $R \lesssim 2 \text{ kpc}$), assuming a conversion factor of $X_{\text{CO}} = 0.8 (\text{K km s}^{-1} \text{ pc}^2)^{-1} M_{\odot}$ and optically thick, thermalised line ratios. Although considerable uncertainty is associated with X_{CO} it is clear that bright SMGs are amongst the most gas-rich systems in the Universe. Comparing with local ULIRGs, we find that SMGs have molecular gas reservoirs on average about four times

greater than even the most CO-luminous ULIRGs. We argue that this is largely due to the evolution in the molecular gas content of the most far-infrared luminous galaxies with redshift.

- In general, the SMGs in our sample have extremely broad line profiles. The median FWHM is $780 \pm 320 \text{ km s}^{-1}$, which is $\gtrsim 3$ times larger than the average CO(1–0) line width of local ULIRGs. The large line widths, and in some cases multiple-peaked CO spectra, together with the vast amounts of molecular gas, suggests that the brightest SMGs are merger events. We argue that the observed gas properties are difficult to reconcile with the scenario witnessed in local ULIRGs where the bulk of the molecular gas resides in a compact circumnuclear disk.

- We find that the median dynamical mass of the SMG sample is $\langle M_{\text{dyn}} \rangle = (1.2 \pm 1.5) \times 10^{11} M_{\odot}$ within the central $\sim 4 \text{ kpc}$. This suggests that the brightest SMGs are amongst the most massive galaxies in the distant Universe, comparable in mass to the most extreme HzRGs and QSOs, rather than being high- z replicas of local ULIRGs. Taking into account the stellar mass component we estimate that the total baryonic mass content of SMGs is $\gtrsim 6 \times 10^{10} M_{\odot}$. Thus we conclude that not only are SMGs very massive baryonic systems, but the baryons can account for a substantial fraction of the total mass in the central regions.

- We have shown that the SMGs exhibit a non-linear correlation between far-infrared and CO luminosity, similar to that observed for local ULIRGs. This not only extends the $L'_{\text{CO}}-L_{\text{FIR}}$ relation to higher luminosities ($L_{\text{FIR}} \sim 10^{12-14} L_{\odot}$) but also shows that it holds at the highest redshifts. The main implication of this is that SMGs have higher $L_{\text{FIR}}/L'_{\text{CO}}$ ratios than ULIRGs, and therefore possibly higher star-formation efficiencies. However, a clearer picture of the star-formation efficiency of SMGs has to await a future systematic survey for high-redshift HCN, which will trace the dense star-forming gas.

- From the inferred molecular gas masses we estimate a typical gas consumption timescale of $\gtrsim 40 \text{ Myr}$. Given the large uncertainties involved, an SMG phase of $\sim 40 \text{ Myr}$ is roughly consistent with the best age estimates of the starbursts in SMGs (Tecza et al. 2004; Smail et al. 2003, 2004), which in turn agree favourably with independent estimates of the duration of the SMG phase obtained by requiring a scenario in which SMGs last 100 – 200 Myrs before going through a $\sim 10 \text{ Myr}$ QSO phase at $z \sim 2$, becoming massive evolved galaxies at $z \sim 1$, followed by a period of passive evolution which sees them ending up as old $\gtrsim L^*$ ellipticals in the present day. Furthermore, the slightly short gas consumption time scales can easily be prolonged by invoking negative feedback processes, and may be indicative of such processes playing an important role in the build-up of massive galaxies.

- From our observations, we place a lower limit on the co-moving number density of massive baryonic systems in the redshift range $z = 2-3.5$ of $n(M_{\text{bar}} \geq 6 \times 10^{10} M_{\odot}) \gtrsim 5.1 \times 10^{-6} \text{ Mpc}^{-3}$ in agreement with results from recent near-infrared/spectroscopic surveys (e.g. Saracco et al. 2004; Glazebrook et al. 2004). Given the substantial uncertainties involved, we find no significant discrepancy between the data and the predicted abundances of massive galaxies at high redshifts.

ACKNOWLEDGMENTS

TRG acknowledges support from the Danish Research Council and from the European Union RTN network, POE. IRS acknowledges support from the Royal Society. AWB acknowledges support from NSF grant AST-0205937, from the Research Corporation and the

Alfred P. Sloan Foundation. JPK thanks Caltech and CNRS for support. We are grateful to Genevieve Soucail and Paola Andreani for letting us use the PdBI CO data for SMM J02396–0134 and ERO J16540+4626, respectively. We also thank Cedric Lacey for providing the GALFORM model predictions. Finally, we thank Dennis Downes for useful comments and suggestions and for allowing us to reproduce the PdBI CO data for SMM J14011+0252.

REFERENCES

- Aalto S., Booth R. S., Black J. H., Johansson L. E. B., 1995, *A&A*, 300, 369.
- Adelberger K. L., Steidel C. C., 2000, *ApJ*, 544, 218.
- Alloin D., Barvainis R., Guilloteau S., 2000, *ApJ*, 528, L81.
- Appleton P. N., Fadda S. T., Marleau F. R., 2004, *ApJS Spitzer Special Issue*, 154, 147.
- Alexander D. M. et al., 2003, *AJ*, 126, 539.
- Alexander D. M., Bauer F. E., Chapman S. C., Smail I., Blain A. W., Brandt W. N., Ivison R. J., 2005, to appear in the Proceedings of the ESO/USM/MPE Workshop on "Multiwavelength Mapping of Galaxy Formation and Evolution", eds. R. Bender and A. Renzini, Venice, Italy. (astro-ph/0401129).
- Andreani P., Casoli F., Gerin M., 1995, *A&A*, 300, 43.
- Andreani P., Cimatti A., Loinard L., Röttgering H., 2000, *A&A*, 354, L1.
- Baker A. J., Tacconi L. J., Genzel R., Lehnert M. D., Lutz D., 2004, *ApJ*, 604, 125.
- Barger A. J., Cowie L. L., Sanders D. B., 1999, *ApJ*, 518, L5.
- Barnes J. E., Hernquist L., 1996, *ApJ*, 471, 115.
- Barvainis R., Tacconi L., Antonucci R., Alloin D., Coleman P., 1994, *Nature*, 371, 586.
- Barvainis R., Maloney P., Antonucci R., Alloin D., 1997, *ApJ*, 484, 695.
- Barvainis R., Alloin D., Guilloteau S., Antonucci R., 1998, *ApJ*, 492, L13.
- Barvainis R., Alloin D., Bremer M., 2002, *A&A*, 385, 399.
- Baugh C. M., Lacey C. G., Frenk C. S., Granato G. L., Silva L., Bressan A., Benson A. J., Cole S., 2004, *MNRAS*, in press, (astro-ph/0406069).
- Beelen A. et al., 2004, *A&A*, 423, 441.
- Bertoldi F., Menten K. M., Kreysa E., Carilli C. L., Owen F., 2000, 24th meeting of the IAU, Joint Discussion 9, Manchester, England.
- Bertoldi, F. et al., 2003, *A&A*, 409, L47.
- Binney J., Tremaine S., 1987, "Galactic Dynamics", Princeton Series on Astrophysics, Princeton University Press.
- Blain A. W., Jameson A., Smail I., Longair M. S., Kneib J.-P., Ivison R. J., 1999, *MNRAS*, 309, 715.
- Blain A. W., Smail I., Ivison R. J., Kneib J.-P., Frayer D. T., 2002, *PhR*, 369, 111.
- Blain A. W., Chapman S. C., Smail I., Ivison R. J., 2004a, *ApJ*, 611, 52.
- Blain A. W., Chapman S. C., Smail I., Ivison R. J., 2004b, *ApJ*, 611, 725.
- Borys C., Chapman S. C., Halpern M., Scott D., 2003, *MNRAS*, 344, 385.
- Braine J., Combes, F., 1992, *A&A*, 264, 433.
- Brown R. L., Vanden Bout P. A., 1991, *AJ*, 102, 1956.
- Carilli C. L. et al., 2002a, *AJ*, 123, 1838.
- Carilli C. L. et al., 2002b, *ApJ*, 575, 145.
- Carilli C. L. et al., 2004, *ApJ*, in press, (astro-ph/0409054).
- Chapman S. C. et al. 2003a, *ApJ*, 585, 57.
- Chapman S. C., Blain A. W., Ivison R. J., Smail I., 2003b, *Nature*, 422, 695.
- Chapman S. C., Windhorst R., Odewahn S., Yan H., Conselice C. J., 2003c, *ApJ*, 599, 92.
- Chapman S. C., Smail I., Windhorst R., Muxlow T., Ivison R. J., 2004, *ApJ*, 611, 732.
- Chapman S. C., Blain A. W., Ivison R. J., Smail I., 2005, *ApJ*, in press, (astro-ph/0412573).
- Cimatti A., Andreani P., Röttgering H., Tilanus R., 1998, *Nature*, 392, 895.
- Cimatti A. et al., 2004, *Nature*, 430, 184.
- Cole S., Aragon-Salamanca A., Frenk C. S., Navarro J. F., Zepf S. E., 1994, *MNRAS*, 271, 781.
- Cole S., Lacey C. G., Baugh C. M., Frenk C. S., 2000, *MNRAS*, 319, 168.
- Cole S. et al., 2001, *MNRAS*, 326, 255.
- Condon J. J., 1992, *ARA&A*, 30, 575.
- Cox P. et al., 2002, *A&A*, 387, 406.
- Daddi E., Cimatti A., Renzini A., 2004, *ApJ*, 600, L127.
- De Breuck C. et al., 2003a, *A&A*, 401, 911.
- De Breuck C., Neri R., Omont A., 2003b, *NewAR*, 47, 285.
- De Breuck C., Downes D., Neri R., van Breugel W., Reuland M., Omont A., Ivison R., 2005, *A&A*, in press, (astro-ph/0411732).
- Devereux N., Taniguchi Y., Sanders D. B., Nakai N., Young J. S., 1994, *AJ*, 107, 2006.
- Dey A., Graham J. R., Ivison R. J., Smail I., Wright G. S., Liu M. C., 1999, *ApJ*, 519, 610.
- Downes D., Solomon P. M., Radford S. J. E., 1995, *ApJ*, 453, L65.
- Downes D., Solomon P. M., 1998, *ApJ*, 507, 615.
- Downes D., Neri R., Wiklind T., Wilner D. J., Shaver, P. A., 1999, *ApJ*, 513, L1.
- Downes D., Solomon P. M., 2003, *ApJ*, 582, 37.
- Drory N., Bender R., Snigula J., Feulner, G., Hopp, U., Maraston C., Hill G. J., Mendes de Oliveira C., 2003, in *The Masses of Galaxies at Low and High Redshift*, ed. R. Bender & A. Renzini (Berlin: Springer). (astro-ph/0201207).
- Dunne L., Eales S., Edmunds M., Ivison R. J., Alexander P., Clements D. L., 2000, *MNRAS*, 315, 115.
- Fontana A., Pozzetti L., Donnarumma I., 2004, *A&A*, 424, 23.
- Ford H. C. et al., 1994, *ApJ*, 435, L27.
- Frayer D. T., Ivison R. J., Scoville N. Z., Yun M., Evans A. S., Smail I., Blain A. W., Kneib J.-P., 1998, *ApJ*, 506, L7.
- Frayer D. T. et al., 1999, *ApJ*, 514, L3L.
- Frayer D. T., Armus L., Scoville N. Z., Blain A. W., Reddy N. A., Ivison R. J., Smail Ian, 2003, *ApJ*, 126, 73.
- Gao Y., Solomon P. M., 1999, *ApJ*, 512, L99.
- Gao Y., Solomon P. M., 2003, *ApJ*, 606, 271.
- Garrett M. A., 2002, *A&A*, 384, L19.
- Genzel R., Baker A. J., Tacconi L. J., Lutz D., Cox P., Guilloteau S., Omont A., 2003, *ApJ*, 584, 633.
- Glazebrook K. et al., 2004, *Nature*, 430, 181.
- Granato G. L., De Zotti G., Silva L., Bressan A., Danese, L., 2004, *ApJ*, 600, 580.
- Greve T. R., Ivison R. J., Papadopoulos P. P., 2003, *ApJ*, 599, 839.
- Greve T. R., Ivison R. J., Papadopoulos P. P., 2004a, *A&A*, 419, 99.
- Greve T. R., Ivison R. J., Bertoldi F., Stevens J. A., Dunlop J. S., Lutz D., Carilli C. L., 2004b, *MNRAS*, 354, 779.
- Guilloteau S., Omont A., McMahon R. G., Cox P., Petitjean P., 1997, *A&A*, 328, L1.

- Guilloteau S., Omont A., Cox P., McMahon R. G., Petitjean P., 1999, *A&A*, 349, 363.
- Guilloteau S., Lucas R., 2000, in "Imaging at Radio through Submillimeter Wavelengths", ed. J. G. Magnum & S. J. E. Radford (San Francisco: ASP), 299.
- Hainline L. J., Scoville N. Z., Yun M. S., Hawkins D. W., Frayer D. T., Isaak K. G., 2004, *ApJ*, 609, 61.
- Holland W. S. et al. 1999, *MNRAS*, 303, 659.
- Hu E. M., Ridgway S. E., 1994, *AJ*, 107, 1303.
- Iono D., Yun M. S., Mihos J. C., 2004, *ApJ*, 616, 199.
- Ivison R. J. et al., 2000, *MNRAS*, 315, 209.
- Ivison R. J., Smail I., Frayer D. T., Kneib J.-P., Blain A. W., 2001, *ApJ*, 561, L45.
- Ivison R. J. et al., 2002, *MNRAS*, 337, 1.
- Kauffmann G., Colberg J. M., Diaferio A., White S. D. M., 1999, *MNRAS*, 303, 188.
- Klamer I. J., Ekers R. D., Sadler E. M., Weiss A., Hunstead R. W., De Breuck C., 2005, *ApJL*, in press, (astro-ph/0501447).
- Kneib J.-P., Neri R., Smail I., Blain A. W., Sheth K., van der Werf P., Knudsen K. K., 2004, *A&A*, 614, L5.
- Knudsen K. K., van der Werf P. P., Jaffe W., 2003, *A&A*, 411, 343.
- Kooiman B. L., Burns J. O., Klypin A. A., 1995, *ApJ*, 448, 500.
- Kreysa E. et al., 1998, *SPIE*, 3357, 319.
- Krips M., Neri R., Eckart A., Martin-Pintado J., Planesas P., Colina L., 2003, "Proceedings of the 4th Cologne-Bonn-Zermatt-Symposium", ed. S. Pfalzner, C. Kramer, C. Straubmeier, and A. Heithausen (Springer Verlag).
- Ledlow M. J., Smail Ian, Owen F. N., Keel W. C., Ivison R. J., Morrison G. E., 2002, *ApJ*, 577, L79.
- Lewis G. F., Carilli C. L., Papadopoulos P. P., Ivison R. J., 2002, *MNRAS*, 330, L15.
- Lilly S. et al., 1998, *ApJ*, 500, L75.
- Martini P., Weinberg D. H., 2001, *ApJ*, 547, 12.
- Mirabel I. F., Sanders D. B., 1989, 340, L53.
- Neri R. et al., 2003, *ApJ*, 597, L113.
- Ohta K., Yamada T., Nakanishi K., Kohno K., Akiyama M., Kawabe R., 1996, *Nature*, 382, 426.
- Oke J. B. et al., 1995, *PASP*, 107, 375.
- Omont A., Petitjean P., Guilloteau S., McMahon R. G., Solomon P. M., Pecontal E., 1996, *Nature*, 382, 428.
- Omont, A., Cox, P., Bertoldi, F., McMahon, R. G., Carilli, C., Isaak, K. G., 2001, *A&A*, 374, 371.
- Page M., Stevens J. A., Ivison R. J., Carrera F. J., 2004, *ApJ*, 611, L85.
- Papadopoulos P. P., Röttgering H. J. A., van der Werf P. P., Guilloteau S., Omont A., Breugel W. J. M., Tilanus R. P. J., 2000, *ApJ*, 528, 626.
- Papadopoulos P. P., Ivison R. J., Carilli C. L., Geraint L., 2001, *Nature*, 409, 58.
- Papadopoulos P. P., Ivison R. J., 2002, *ApJ*, 564, L9.
- Planesas P., Martin-Pintado J., Neri R., Colina L., 1999, *Science*, 286, 2493.
- Ravindranath S. et al., 2004, *ApJ*, 604, L9.
- Richards G. T., Vanden Berk D. E., Reichard T. A., Hall P. B., Schneider D. P., SubbaRao M., Thakar A. R., York D. G., 2002, *AJ*, 124, 1.
- Rickard L. J., Palmer P., Morris M., Turner B. E., Zuckerman B., 1975, *ApJ*, 199, L75.
- Rickard L. J., Harvey P. M., 1984, *AJ*, 89, 1520.
- Rigopoulou D., Spoon H. W. W., Genzel R., Lutz D., Moorwood A. F. M., Tran Q. D., 1999, *AJ*, 118, 2625.
- Saracco P. et al., 2004, *A&A*, 420, 125.
- Sakamoto K., Scoville N. Z., Yun M. S., Crosas M., Genzel R., Tacconi L. J., 1999, *ApJ*, 514, 68.
- Sanders D. B., Mirabel I. F., 1985, *ApJ*, 298, L31.
- Sanders D. B., Scoville N. Z., Young J. S., Soifer B. T., Schloerb F. P., Rice W. L., Danielson G. E., 1986, *ApJ*, 305, L49.
- Sanders D. B., Scoville N. Z., Soifer B. T., 1991, *ApJ*, 370, 158.
- Scott S. E. et al., 2002, *MNRAS*, 331, 817.
- Scoville N. Z., Yun M. S., Windhorst R. A., Keel W. C., Armus L., 1997, *ApJ*, 485, L21.
- Seaquist E. R., Ivison R. J., Hall P. J., 1995, *MNRAS*, 276, 867.
- Sheth K., Blain A. W., Kneib J.-P., Frayer D. T., van der Werf P., Knudsen, K. K., 2004, *ApJ*, 614, L5.
- Simpson C., Dunlop J. S., Eales S. A., Ivison R. J., Scott S. E., Lilly S. J., Webb T. M. A., 2004, *MNRAS*, 353, 179.
- Smail I., Ivison R. J., Blain A. W., 1997, *ApJ*, 490, L5.
- Smail I., Ivison R. J., Kneib J.-P., Cowie L. L., Blain A. W., Barger A. J., Owen F. N., Morrison, G., 1999, *MNRAS*, 308, 1061.
- Smail I., Ivison R. J., Blain A. W., Kneib J.-P., 2002, *MNRAS*, 331, 495.
- Smail I., Chapman S. C., Ivison R. J., Blain A. W., Takata T., Heckman T. M., Dunlop J. S., Sekiguchi K., 2003, *MNRAS*, 342, 1185.
- Smail I., Chapman S. C., Blain A. W., Ivison R. J., 2004, *ApJ*, 616, 71.
- Solomon P. M., Sage L. J., 1988, *ApJ*, 334, 613.
- Solomon P. M., Downes D., Radford S. J. E., 1992a, *Nature*, 356, 318.
- Solomon P. M., Downes D., Radford S. J. E., 1992b, *ApJ*, 398, L29.
- Solomon P. M., Downes D., Radford S. J. E., Barrett J. W., 1997, 478, 144.
- Solomon P. M., Vanden Bout P., Carilli C. L., Guelin M., 2003, *Nature*, 426, 636.
- Somerville R. S., Primack J. R., Faber S. M., 2001, *MNRAS*, 320, 504.
- Soucail G., Kneib J.-P., Bezecourt J., Metcalfe L., Altieri B., Le Borgne J. F., 1999, *A&A*, 343, L70.
- Spergel D. N. et al., 2003, *ApJS*, 148, 175.
- Swinbank A. M., Smail I., Chapman S. C., Blain A. W., Ivison R. J., Keel W. C., 2004, *ApJ*, 617, 64.
- Tacconi, L. et al., 2005, *ApJ*, submitted.
- Tecza M. et al., 2004, *ApJ*, 604, L109.
- Walter F. et al., 2003, *Nature*, 424, 406.
- Webb T. M. et al., 2003, *ApJ*, 587, 41.
- Weiss A., Henkel C., Downes D., Walter F., 2003, *A&A*, 409, L41.
- White S. D. M., Frenk C. S., 1991, *ApJ*, 379, 52.
- Wilner D. J., Zhao, J.-H., Ho P. T. P., 1995, *ApJ*, 453, L91.
- Wyse R. F. G., Gilmore G., Franx M., 1997, *ARA&A*, 35, 637.
- Yao L., Seaquist E. R., Kuno N., Dunne L., 2003, *ApJ*, 588, 771.
- Young J. S., Kenney J., Lord S. D., Schloerb F. P., 1984, *ApJ*, 287, L65.
- Young J. S., Schloerb F. P., Kenney J. D., Lord S. D., 1986, *ApJ*, 304, 443.
- Yun M. S., Reddy N. A., Condon J. J., 2001, *ApJ*, 554, 803.

This paper has been typeset from a \LaTeX file prepared by the author.